

NAVAL POSTGRADUATE SCHOOL

Monterey, California



19980102 155

THESIS

**CONSTRUCTION OF A CONTINUOUS WAVE
FREQUENCY MODULATION SENSITIVE
LASER RADAR FOR USE IN
TARGET IDENTIFICATION**

by

James V. Day

March, 1997

Thesis Advisor:
Second Reader:

Robert C. Harney
Andres Larraza

Approved for public release; distribution is unlimited.

DTIC QUALITY INSPECTED

REPORT DOCUMENTATION PAGE			Form Approved OMB No. 0704-0188	
Public reporting burden for this collection of information is estimated to average 1 hour per response, including the time for reviewing instruction, searching existing data sources, gathering and maintaining the data needed, and completing and reviewing the collection of information. Send comments regarding this burden estimate or any other aspect of this collection of information, including suggestions for reducing this burden, to Washington Headquarters Services, Directorate for Information Operations and Reports, 1215 Jefferson Davis Highway, Suite 1204, Arlington, VA 22202-4302, and to the Office of Management and Budget, Paperwork Reduction Project (0704-0188) Washington DC 20503.				
1. AGENCY USE ONLY (Leave blank)	2. REPORT DATE March 1997	3. REPORT TYPE AND DATES COVERED Master's Thesis		
4. CONSTRUCTION OF A CONTINUOUS WAVE FREQUENCY MODULATION SENSITIVE LASER RADAR FOR USE IN TARGET IDENTIFICATION		5. FUNDING NUMBERS		
6. AUTHOR(S) Day, James V.				
7. PERFORMING ORGANIZATION NAME(S) AND ADDRESS(ES) Naval Postgraduate School Monterey CA 93943-5000		8. PERFORMING ORGANIZATION REPORT NUMBER		
9. SPONSORING/MONITORING AGENCY NAME(S) AND ADDRESS(ES)		10. SPONSORING/MONITORING AGENCY REPORT NUMBER		
11. SUPPLEMENTARY NOTES The views expressed in this thesis are those of the author and do not reflect the official policy or position of the Department of Defense or the U.S. Government.				
12a. DISTRIBUTION/AVAILABILITY STATEMENT Approved for public release; distribution is unlimited.			12b. DISTRIBUTION CODE	
13. ABSTRACT (maximum 200 words) This thesis covers the theory, design and construction of a continuous wave (CW) frequency modulation sensitive laser radar. Using a commercially available CO ₂ laser, optics and electronics, a CW frequency modulation sensitive laser radar was constructed and tested under laboratory conditions. The theory of each component in the laser radar is covered as well as the configuration and design of the radar. Design of a target that enabled measurement of the laser radar's capabilities was also completed. The laser radar was able to accurately measure a target's vibrational frequency and amplitude for amplitudes greater than 40 nm. The theoretical range of the designed laser radar is over 6 km. An improved optical design that allows a theoretical range of over 9 km is also presented. Applications of target identification are discussed.				
14. SUBJECT TERMS: Laser Radar, Acousto-optic Modulation, Non-Cooperative Target Identification, Vibrations.			15. NUMBER OF PAGES 98	
			16. PRICE CODE	
17. SECURITY CLASSIFICATION OF REPORT Unclassified	18. SECURITY CLASSIFICATION OF THIS PAGE Unclassified	19. SECURITY CLASSIFICATION OF ABSTRACT Unclassified	20. LIMITATION OF ABSTRACT UL	

Approved for public release; distribution is unlimited.

**CONSTRUCTION OF A CONTINUOUS WAVE
FREQUENCY MODULATION SENSITIVE
LASER RADAR FOR USE IN
TARGET IDENTIFICATION**

James V. Day
Captain, United States Army
BS, San Jose State University, 1984

Submitted in partial fulfillment
of the requirements for the degree of

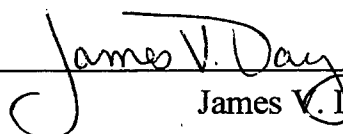
MASTER OF SCIENCE IN APPLIED PHYSICS

from the

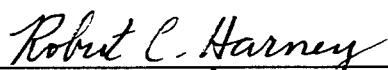
NAVAL POSTGRADUATE SCHOOL

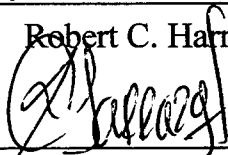
March 1997


Author:


James V. Day

Approved by:


Robert C. Harney, Thesis Advisor


Andres Larraza, Second Reader


Anthony A. Atchley, Chairman
Department of Physics

DISCLAIMER

The use or mention of the commercial equipment in this thesis does not in any way constitute an endorsement by the Naval Postgraduate School or the United States Navy.

ABSTRACT

This thesis covers the theory, design and construction of a continuous wave (CW) frequency modulation sensitive laser radar. Using a commercially available CO₂ laser, optics and electronics, a CW frequency modulation sensitive laser radar was constructed and tested under laboratory conditions. The theory of each component in the laser radar is covered as well as the configuration and design of the radar. Design of a target that enabled measurement of the laser radar's capabilities was also completed. The laser radar was able to accurately measure a target's vibrational frequency and amplitude for amplitudes greater than 40 nm. The theoretical range of the designed laser radar is over 6 km. An improved optical design that allows a theoretical range of over 9 km is also presented. Applications of target identification are discussed.

TABLE OF CONTENTS

I. INTRODUCTION	1
A. PURPOSE.....	1
B. BACKGROUND.....	1
C. BASIC CONCEPTS.....	3
D. POSSIBLE APPLICATIONS FOR LASER RADAR.....	5
II. THEORY	7
A. DETECTING A TARGET'S POSITIONAL CHANGES.....	7
1. The Purpose of Frequency Shifting in Laser Radar	8
2. Intensity Modulation Due to Vibrational Amplitude.....	10
3. The Importance of Coherence, Coincidence and Parallelism	11
B. CO ₂ LASER THEORY	13
1. The CO ₂ Excitation Process	13
2. The Emission Process.....	17
3. Feedback, Oscillation and Amplification of Laser Light	19
4. Line shape, Cavity Modes and Lasing Threshold.	20
5. Gaussian Beams and Hermite-Gaussian Mode Patterns.....	23
6. Laser Efficiency.	25
C. LENSES AND BEAM SPLITTERS.....	26
1. Lenses.....	26
2. Beam Splitters.....	28
D. ACOUSTO-OPTIC MODULATION.....	30
E. DETECTORS.....	33
F. LASER RADAR EQUATIONS.....	36
III. EXPERIMENTAL SET UP	39
A. SAFETY	39
1. Class IV Laser Room.....	40
2. Laser Safety Distances	41
B. LASER SELECTION AND SETUP.....	42
1. Synrad Laser	42
2. Laser Cooling	44
C. OPTICAL BREADBOARD	45
D. ACOUSTO-OPTIC MODULATOR CONFIGURATION.....	46
E. LENS SETUP	47
1. Design Considerations.....	47
2. Lens Mounts	48
3. Coincidence and Parallelism of the Beams	49
F. TARGET CONFIGURATION.....	52
1. Piezoelectronics	52
2. Piezoelectric Response Times.....	54
3. Piezoelectric Stack Strength Limitations.....	55

4. Piezoelectric Current Requirements.....	55
G. ELECTRONICS	57
H. DATA RECORDING.....	60
IV. OBSERVATIONS, ANALYSIS AND RECOMMENDATIONS	61
A. OBSERVATIONS	61
B. CONCLUSIONS AND RECOMMENDATIONS.....	69
1. Measurement Capabilities.....	69
2. System Improvements	70
APPENDIX – LASER SAFETY PROCEDURES.....	73
LIST OF REFERENCES.....	77
INITIAL DISTRIBUTION LIST.....	81

LIST OF FIGURES

Figure 1-1 Vehicle Vibration Sources (Harney, 1993).....	3
Figure 1-2 Coherent Detection Schemes (Harney, 1993).....	4
Figure 1-3 Possible Applications for Laser Radar.....	6
Figure 2-1 Laser Vibration Sensing (Harney, 1993)	9
Figure 2-2 Coherence of Light (Wilson, 1989).....	11
Figure 2-3 Angular Misalignment and Coherence (Scruby, 1990).....	12
Figure 2-4 Synrad Laser Cross-Section (Synrad, 1996).....	14
Figure 2-5 CO ₂ Energy Level Diagram (Hawkes, 1995).....	15
Figure 2-6 Effects of Radiation on an Atom (Verdeyen, 1995).....	18
Figure 2-7 Laser Configuration.....	19
Figure 2-8 Laser Frequency Control	22
Figure 2-9 Hermite-Gaussian Modes (Siegman, 1986)	24
Figure 2-10 Synrad Laser Efficiency	25
Figure 2-11 Synrad Laser Power Output.....	26
Figure 2-12 Lens Optics	27
Figure 2-13 Lenses	28
Figure 2-14 Beam Splitters And Partial Reflectors	29
Figure 2-15 Acousto-Optic Modulator.....	31
Figure 2-16 Detector Circuit Layout.....	35
Figure 2-17 CNR Vs. Range (km)	38
Figure 3-1 Interlock Design.....	40
Figure 3-2 Synrad Laser Physical Features Diagram (Synrad, 1996).....	43
Figure 3-3 Laser Power Cooling Configuration.....	44
Figure 3-4 Acousto-Optic Modulator Configuration	46
Figure 3-5 Optical Configuration	47
Figure 3-6 Optical Alignment.....	49
Figure 3-7 Beam Alignment.....	50
Figure 3-8 Beam Alignment on the Detector	52

Figure 3-9 Piezoelectric Displacement vs. Voltage (Thor Labs, 1996).....	53
Figure 3-10 Target Design.....	56
Figure 3-11 Electronic Configuration.....	57
Figure 3-12 Frequency Discrimination (Miteq, 1996).....	59
Figure 4-1 Response of the Vibrating Target	62
Figure 4-2 Response with Target Turned Off.....	63
Figure 4-3 Response with Target and Laser Off.....	64
Figure 4-4 Power Surge.....	65
Figure 4-5 Laser Radar Return from a Target Vibrating at 400 Hz and 40 nm Amplitude	66
Figure 4-6 Laser Radar Return from a Target Vibrating at 400 Hz and 1 μ m Amplitude.	67
Figure 4-7 Laser Radar Return from a Target Vibrating at 500 Hz and 1.74 μ m Amplitude.	68
Figure 4-8 Improved Laser Radar Design	71

LIST OF SYMBOLS

a	amplitude of target vibration
A	detector area
A_c	interference coefficient
A_{21}	spontaneous emission coefficient
α	atmospheric attenuation coefficient
B	electronic bandwidth
β	maximum efficiency heterodyne angle
C	capacitance of the piezoelectric stack
c	speed of light
D	total distance the light beam has to travel to the target and back
D	transmitting optics diameter
d	distance to the target
D_b	beam width
E_g	energy gap
E_1, E_2	amplitude of the electric field (1, 2) at a given point
E_{10}, E_{20}	maximum amplitudes of the electric fields
ϵ_T, ϵ_R	transmit (receive) path optics efficiency
f	focal length of a lens
f_i	maximum frequency from current relationships
f_l	frequency of the laser
f_r	new system resonant frequency
f_r	the resonant frequency of the piezoelectric stack alone
f_m	Doppler shift caused by target motion
f_s	frequency shift caused by the modulator
f_s	maximum frequency from strength relations
f_t	frequency of target vibration
Δf	electrical bandwidth
G	photoconductive gain

$g(\nu)$	lineshape
g_1	number ways that the CO ₂ molecule can have energy level 1
g_2	number ways that the CO ₂ molecule can have energy level 2
G_o	gain factor
$\gamma(\nu)$	gain coefficient
h	Plank's constant
I	current applied to the piezoelectric stack
I	intensity of light
J_n	Bessel Function of order n
ΔJ	change in rotational energy level
L	cavity length, optical path length
l	length of gain medium in the cavity
λ	wavelength of emitted radiation
λ_c	cut off wavelength
Λ	acoustic wavelength
k	Boltzman's constant
m	order of diffraction
m_p	mass of the piezoelectric stack
M_r	mass of the retro-reflector
NEP	noise equivalent power
N_1	number of CO ₂ molecules energy level 1 per unit volume
N_2	number of CO ₂ molecules energy level 2 per unit volume
η_D	detector quantum efficiency
η_h	heterodyne efficiency
n_m	refractive index of a medium
P	incident power
ϕ_1, ϕ_2	phase of the electric field (1, 2) at a given point
ρ	target reflectivity
R	range to the target

R	responsivity
r_1, r_2	radius of curvature (1 and 2)
R_1, R_2	reflectance of mirrors (1 and 2)
r_T	target radius
S	fringe spacing
S_l	limiting strength of the piezoelectric stack
t	time
T	absolute temperature
θ_B	Bragg angle
u	target velocity
v_a	acoustic velocity
V_D	voltage applied to the piezoelectric stack
V_n	rms. of the noise voltage
V_s	rms. of the signal voltage
ν	frequency of light, vibrational energy level
$\Delta \nu$	change in vibrational energy level
$\Delta \nu$	cavity mode frequency separation
w_0	beam waist radius
$w(z)$	spot size of the laser beam at distance z
z	distance laser beam traveled
z_0	characteristic length parameter of a Gaussian beam

I. INTRODUCTION

A. PURPOSE

Target identification has become increasingly important in today's complex battlefield environment. The U.S. military is currently investigating several methods of identifying friend or foe on the battlefield. Non-cooperative target identification is currently under investigation as a possible means of identifying vehicles on the battlefield.

The purpose of this thesis is to present the theory, design and construction of a laser radar with the ability to measure a target's vibrations. When combined with a signal processing unit, this system would have the capability of performing non-cooperative target identification at ranges typical of modern ground combat. This thesis shows how a 10 Watt CO₂ laser radar system can detect a target's vibrations at theoretical ranges over 6 km. We constructed and tested the laser radar in a laboratory environment using off the shelf commercial components. The theory of vibration detection and measurement using a laser radar is developed to show that both frequency and amplitude measurements are possible with the laser radar. The theory behind each component within the basic laser radar system is presented. A target capable of controlled vibration was constructed to allow measurement of the laser radar's capabilities.

B. BACKGROUND

Target identification is critical to success on the modern battlefield. Recent military experience has shown that despite the efforts to train personnel in vehicle identification fratricide is still a common occurrence. Public opinion increasingly influences modern warfare and casualties influence public opinion. The military is therefore working to find ways to improve its ability to recognize friend from foe. Current efforts include the U.S. Army's work on a cooperative system called the Battlefield Combat Identification System (BCIS) and better positional knowledge through use of the global positioning system (GPS).

Almost all military equipment emits energy in the form of acoustic waves. These waves can travel through the material that make up the equipment. Solids, liquids and gases can all propagate acoustic waves. In a solid there are two types of acoustic waves: longitudinal and transverse. For longitudinal waves, the particle displacement is in the direction parallel to the axis of propagation, while for transverse waves the displacement is in the direction perpendicular to the axis of propagation. These waves can reach the surface of the material where they can be detected. According to the frequency range, acoustic waves are (Scruby, 1990):

- Infrasonic Range <50 Hz
- Audible Range 50 Hz - 20 kHz
- Ultrasonic Range 20 kHz - 2 GHz.

Using a target's acoustic signature to classify and identify vehicle type has been a common use in naval sonar systems. Because of the lower attenuation in water, acoustic noise from vehicles can be intercepted and analyzed at greater distances in water than in air. Attempts at detecting audible acoustic waves in air at long ranges have been tried as early as World War II. The Japanese attempted to detect and identify incoming aircraft by their acoustic signals with little success.

Soldiers can easily distinguish a HMMWV from an M1 tank just by the way they sound. With a little experience, it becomes easy to distinguish the difference between most military vehicles based on their acoustic signatures. Mechanics have often been able to determine mechanical problems just by listening to a vehicle's sounds. So ground vehicle identification by acoustic signature is possible. It would be advantageous if detection of the sound or acoustic signature from these vehicles at long distances were possible.

Figure 1-1 shows the sources of vibrations in military equipment. Not all of the vibrations are in the audible range; therefore it would be advantageous for identification purposes if the system had as wide a detection range as possible.

C. BASIC CONCEPTS

The advent of lasers has given us the tool to detect target vibrations at long distances. Laser radar has several distinct advantages over traditional radar including greater angular resolution, range resolution and velocity resolution. By using the principles of interference and superposition it is possible to detect the target's vibrations at long distances. The basic concept for detecting vibrations in a target involves measuring the relative phase between two electromagnetic waves of the same frequency and polarization. One wave, called the reference wave or local oscillator wave, travels a fixed distance while the other wave travels to the target. When the second wave returns, it is added to the reference wave. The result is an interference term that has a strength that is a function of

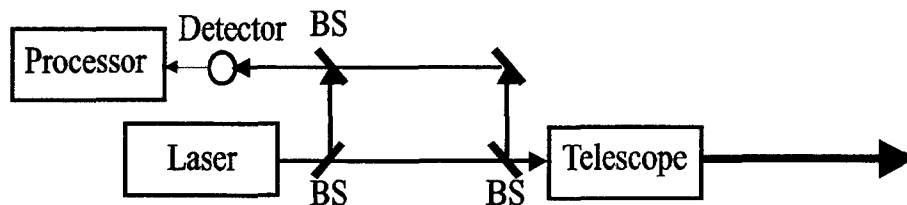
- | | |
|--|---|
| <ul style="list-style-type: none">• Rotary-Wing Aircraft<ul style="list-style-type: none">– Direct Driven Vibrations and Harmonics<ul style="list-style-type: none">• Engine RPM• Main Tail Rotor RPM<ul style="list-style-type: none">• Blade Passing– High-Frequency Skin Vibrations• Fixed Wing Aircraft<ul style="list-style-type: none">– Direct Driven Vibrations and Harmonics<ul style="list-style-type: none">– Structural Vibrations– High Frequency Skin Vibrations | <ul style="list-style-type: none">• Ground Vehicles<ul style="list-style-type: none">– Direct Driven Vibrations and Harmonics<ul style="list-style-type: none">• Cylinder Firing• Engine RPM• Drive Train RPM<ul style="list-style-type: none">• Wheel RPM• Tread Slapping• Auxiliary Equipment Vibrations– Rigid Body Modes (Roll, Pitch, Yaw, Heave)– High Frequency Skin Vibrations• Missiles<ul style="list-style-type: none">– Structural Vibrations– High Frequency Skin Vibrations |
|--|---|

Figure 1-1 Vehicle Vibration Sources (Harney, 1993)

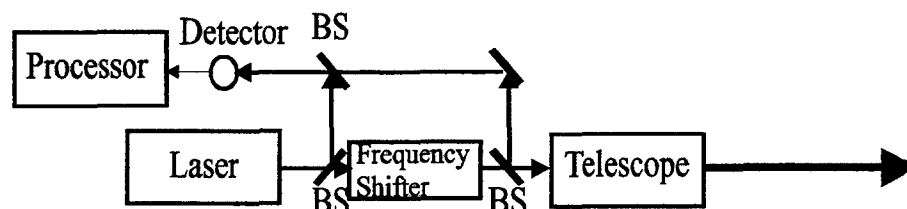
the relative phase between the two waves. This relative phase changes with the target's change in position.

The relative phase is inversely proportional to the wavelength of the electromagnetic waves used. Smaller wavelength waves are the best for small distance resolution. Thus high frequency lasers are much more accurate in determining motion associated with vibration in a target. This process of combining electromagnetic waves is often called coherent detection. It is also often called the heterodyne process. There are several configurations of laser radar that use the coherent detection scheme. Figure 1-2 shows three of these configurations.

a) Homodyne



b) Offset Homodyne



c) Heterodyne

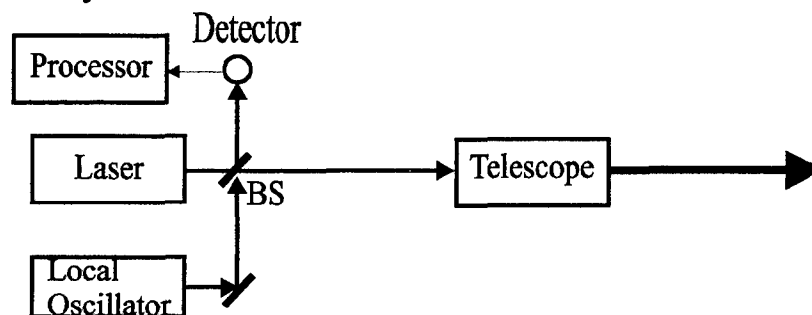


Figure 1-2 Coherent Detection Schemes (Harney, 1993)

Figure 1-2a shows the homodyne configuration. This configuration is the simplest of the three configurations, but it is limited in its ability to detect the direction of motion. Figure 1-2b is the offset homodyne configuration that uses a frequency shifter to enable the radar to detect the direction of motion. The final configuration is the most expensive since it actually has two separate lasers. The local oscillator's frequency must be precisely controlled. This allows an adjustable frequency shift that has additional benefits as we will see later. Our laser radar design will follow the offset homodyne design. This configuration can be constructed at a moderate price.

D. POSSIBLE APPLICATIONS FOR LASER RADAR

The interest in the military applications of laser radar's ability to detect vibrations at a distance depends on the service. The most recent study was conducted for the U.S. Army Communications and Electronics Command by Schwartz Electro-Optics Inc. (Schwartz, 1994). This study provided the Army with a technical report on a working laser radar model that could detect the power stroke frequency of several commercial vehicles. European Studies have shown that helicopters can be identified with 90% accuracy (Kranz, 1989). This signal is then processed to determine the type of aircraft targeted.

Figure 1-3 shows these applications as well as some other possible applications. The laser radar's ability to detect small amplitude vibrations gives it the capability to detect hidden targets. For example, if a submarine is operating above the thermal layer, a satellite with the laser radar system could detect the acoustic waves that reach the ocean's surface. The signals could be sent to a signal processing unit on the ground that would take up the challenging task of filtering out the wave effects and other noise. Hidden enemy vehicles would not have to be in direct line of sight to be detected. These vehicles would transmit their characteristic vibrations into the earth. Nearby reflective objects would begin to vibrate. These vibrations could then be detected and the signal analyzed.

The following chapters describe the theory and construction of an experimental laser radar that will allow the Naval Postgraduate School Physics department to investigate the use of laser radar in these applications.

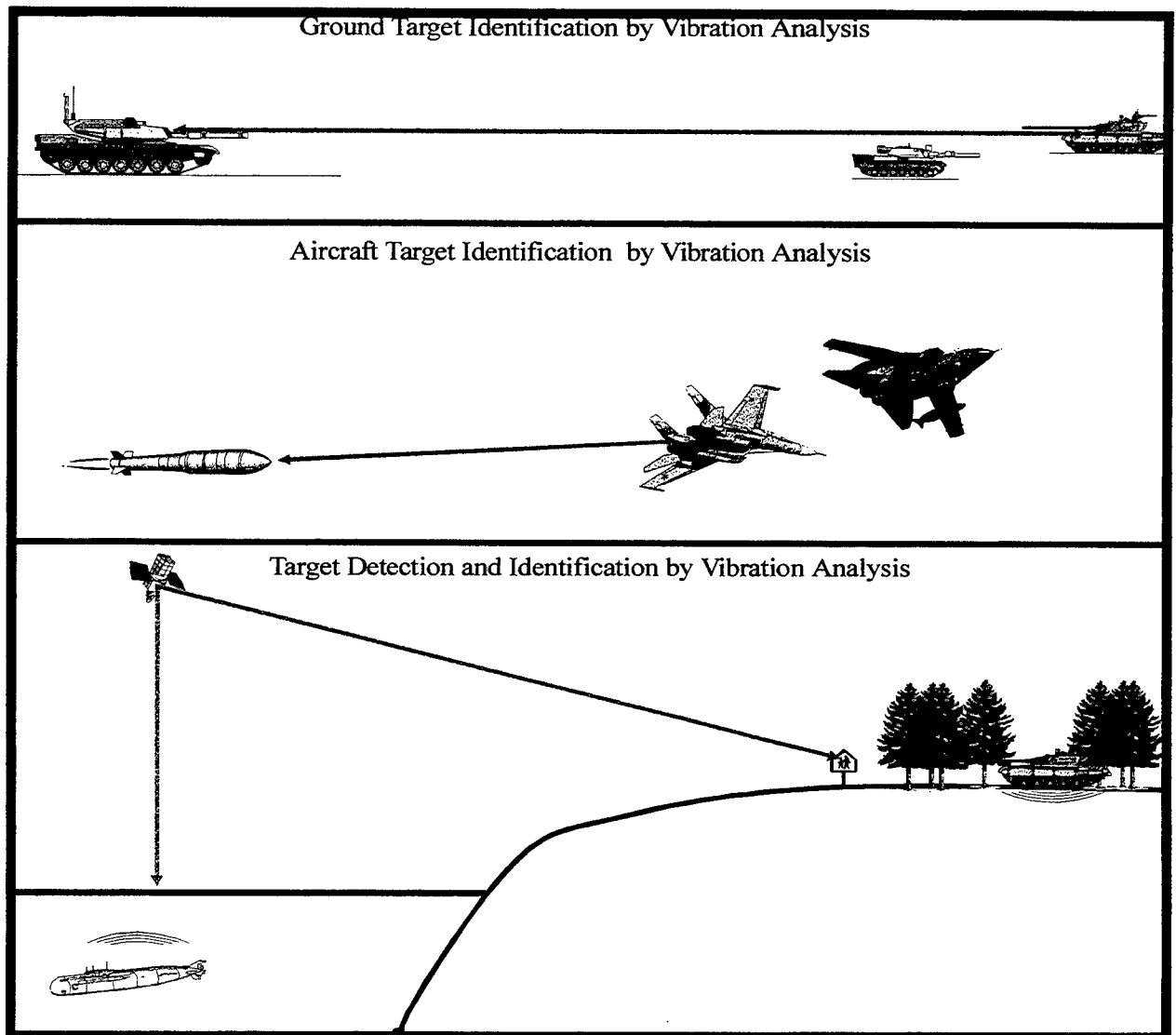


Figure 1-3 Possible Applications for Laser Radar

II. THEORY

In this section we present the principles of a laser radar. Beginning with heterodyne concepts, we will show how the interference between two light beams can be used to detect and measure motion in a target. We will describe each component in the laser radar. Finally, we will cover radar and detection theory as it pertains to our laser radar.

A. DETECTING A TARGET'S POSITIONAL CHANGES

The change in a target's position can be detected with great accuracy using the principle of superposition of light beams. If we add two beams of the same frequency and polarization, interference of the electromagnetic field at a given point will result. The relative phase difference between the two light beams determines whether constructive or destructive interference occurs. C. B. Scruby's book on laser ultrasonics contains a description of the use of the interference principle in laser vibration detection. (Scruby, 1990) Consider the electromagnetic field of two light beams at a point given by

$$E_1 = E_{10} \cos(2\pi\nu t + \phi_1) \quad \text{and} \quad E_2 = E_{20} \cos(2\pi\nu t + \phi_2), \quad (2-1)$$

where E_1 and E_2 are the amplitudes of the electric fields at a given point, ϕ_1 and ϕ_2 are the phases of the two electric fields at a given point, and E_{10} and E_{20} are the maximum amplitudes of the electric fields. The frequency of light is represented by ν and t represents time.

The total fields is

$$\begin{aligned} E_{\text{Total}} = E_1 + E_2 = & (E_{10} \cos(\phi_1) + E_{20} \cos(\phi_2))\cos(2\pi\nu t) \\ & - (E_{10} \sin(\phi_1) + E_{20} \sin(\phi_2))\sin(2\pi\nu t). \end{aligned} \quad (2-2)$$

We are interested in detecting the change in the light as the target's position changes. Most detectors respond to the intensity of light I , which is proportional to the average of the square of the total electrical field. Absorbing the proportionality constant into I and squaring Equation (2-2) yields

$$I_{\text{Total}} = I_1 + I_2 + 2(I_1 I_2)^{1/2} \cos(\phi_1 - \phi_2). \quad (2-3)$$

The last term, $2(I_1 I_2)^{1/2} \cos(\phi_1 - \phi_2)$, is the interference term. If we fix the distance one of the beams has to travel to the detector, its phase will remain constant (let ϕ_2 equal a constant, and for simplicity let it equal zero). This reference beam is often called the local oscillator. The total distance D , that the second light beam has to travel to the target and back to the detector accounts for the second phase term, ϕ_2 which is proportional to the number of wavelengths on the path D . The relationship between the light's phase and distance to the target is

$$\phi_1 = 2\pi \frac{D}{\lambda} = 4\pi \frac{d}{\lambda}. \quad (2-4)$$

We assume that the distance to the target d , is equal to half the round trip distance, D . The symbol λ represents the wavelength of the light. Let the target remain stationary at normal incidence but vibrate in a sinusoidal fashion with an amplitude a and frequency f_t . If the displacement of the target $d = a \sin(2\pi f_t t)$ the phase relationship becomes

$$\phi_1 = 4\pi \frac{a}{\lambda} \sin(2\pi f_t t). \quad (2-5)$$

The total intensity becomes

$$I_{\text{Total}} = I_1 + I_2 + 2(I_1 I_2)^{1/2} \cos(4\pi \frac{a}{\lambda} \sin(2\pi f_t t)). \quad (2-6)$$

The vibrating surface causes a variation in the total intensity directly related to the target's frequency of vibration. The displacement of the surface also modulates the amplitude of the total intensity.

1. The Purpose of Frequency Shifting in Laser Radar

The problem with this set up is that it is hard to determine the direction of displacement. Movement towards the detector can result in the same intensity as movement away from the detector. To overcome this problem designers shift the frequency of the light beam directed at the target by a frequency f_s . The phase of the light beam that has been shifted and reflected off the vibrating target becomes

$$\phi_1 = 2\pi f_s t + 4\pi \frac{a}{\lambda} \sin(2\pi f_t t). \quad (2-7)$$

The total intensity becomes

$$I_{\text{Total}} = I_1 + I_2 + 2(I_1 I_2)^{1/2} \cos(2\pi f_s t + 4\pi \frac{a}{\lambda} \sin(2\pi f t)). \quad (2-8)$$

The total intensity will vary centered on the shift frequency as long as $2\pi f_s t \geq 4\pi \frac{a}{\lambda} \sin(2\pi f t)$.

The above discussion centered in on the target's vibration and how it shifts the frequency of the reflected light. A target's translational velocity can Doppler shift the incident light beam as well. Figure 2-1 shows how Doppler frequency shifting occurs when the light beam is reflected off a target that is moving. For the case of a target moving at a velocity u the frequency shift in the light beam is

$$f_m = \frac{2u}{\lambda} \cos \theta. \quad (2-9)$$

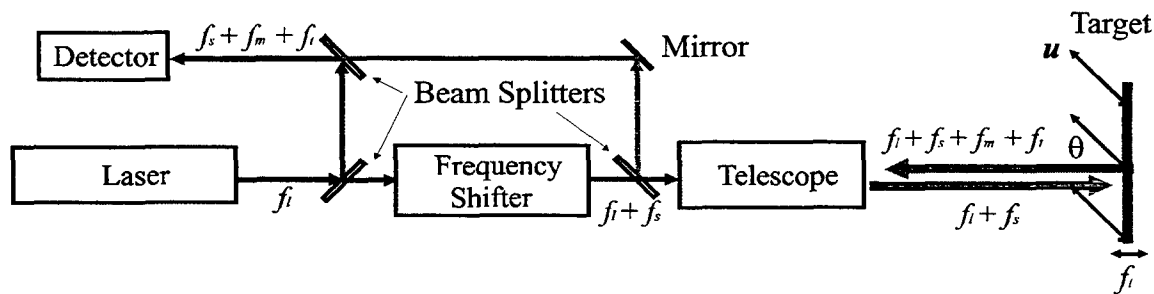


Figure 2-1 Laser Vibration Sensing (Harney, 1993)

This frequency shift is in addition to the vibrational frequency shift. Their combined effects must be considered when selecting a shift frequency f_s . If the target is moving fast enough the Doppler shift from translational motion can negate the frequency shift of the laser radar and result in an error in frequency measurement. If the target is moving directly away from the radar at a velocity of 500 kph the resulting frequency shift is over 26 MHz for a laser with $\lambda = 10.6 \mu\text{m}$. Our laser radar uses a commonly available acousto-optic modulator (AOM) to shift the frequency of the light beam. This frequency shifter is capable of a 30 MHz frequency shift. Theoretically our laser radar could handle target speeds of up to 572 kph. However, at this velocity the target's vibration becomes

harder to detect since we have now lost the frequency shift benefits. Additionally, filtering and amplification used to process the signal from the detector will need to have a wide bandwidth or be adjustable to match the shift in frequency due to the target's velocity.

2. Intensity Modulation Due to Vibrational Amplitude

Intensity modulates as a function of the amplitude of vibration and the vibration frequency. If we concentrate on only the variation of the intensity and arbitrarily let the interference coefficient equal A_c , equation 2-8 becomes

$$I = A_c \cos(2\pi f_s t + 4\pi \frac{a}{\lambda} \sin(2\pi f_t t)), \quad (2-10)$$

analogous to the expression of a FM signal. (Haykin, 1994, Shrader, 1991 and Taub, 1986) The modulation index in our equation is $4\pi \frac{a}{\lambda}$. If the amplitude of the target vibration is large compared to our wavelength we have in essence wide band FM. If the amplitude of our target's vibration is small it fits into what is called narrow band frequency modulation. Equation 2-10 can be expanded in terms of Bessel functions to produce a well known system of sideband frequencies $f_s \pm n f_t$ with intensity amplitudes proportional to $J_n(4\pi \frac{a}{\lambda})$ where J_n is a Bessel function of order n (Scruby, 1990). For small displacements, where the amplitude of vibration is less than half the wavelength of the light beam used, the important sidebands are reduced to $f_s \pm f_t$. This corresponds to the first order Bessel function and the variation in intensity is proportional to $4\pi \frac{a}{\lambda}$. Vibrational amplitudes of greater than half a wavelength will have additional sidebands that show up. Each of these side bands has an intensity proportional to its corresponding higher order Bessel function. The result is a non-linear variation in intensity for vibrational amplitudes of greater than half a wavelength.

3. The Importance of Coherence, Coincidence and Parallelism

Several factors are important in setting up interference at the detector. The light beams used should be as coherent as possible. Figure 2-2a shows perfectly coherent light. Ideally both light beams used to set up the interference effects would initially have the same coherence. Then any change in the relative phase of the two light beams would be due to target motion and vibration. Figure 2-2b shows a light beam that is spatially

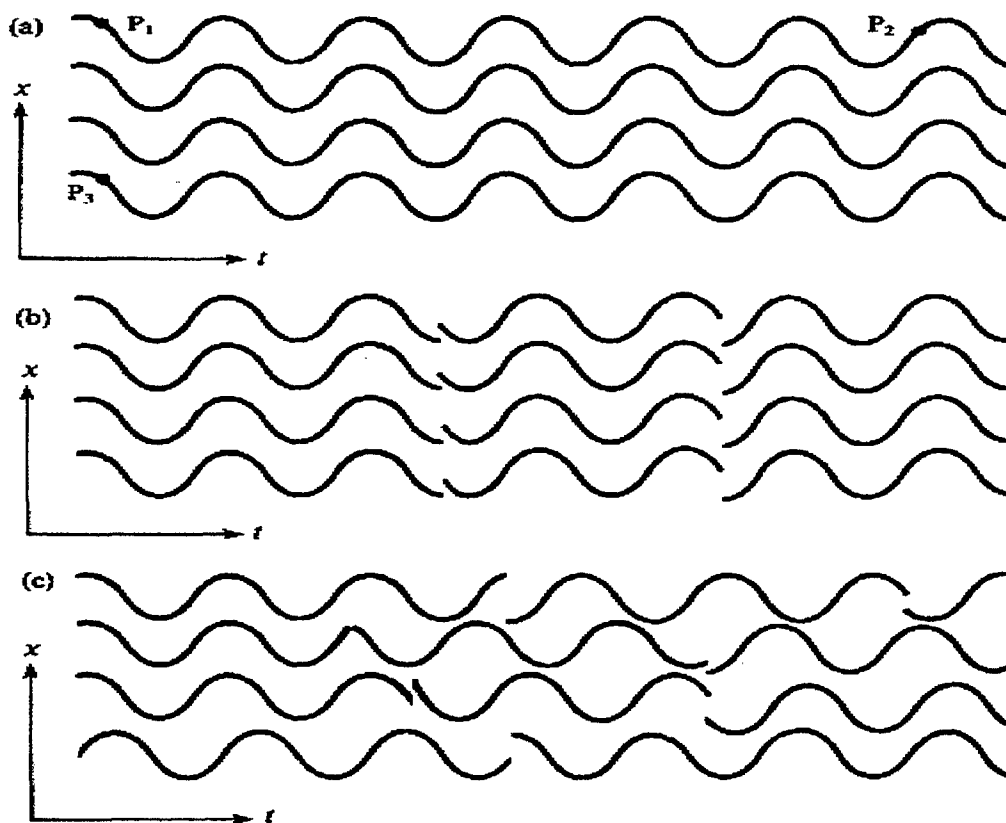


Figure 2-2 Coherence of Light (Wilson, 1989)

coherent but not temporally coherent. The light waves simultaneously change phase by an identical amount. This makes velocity and vibrations harder to determine. Figure 2-2c shows incoherent light. Fortunately lasers produce very coherent light. This quality makes lasers an ideal source for the light beams.

The two light beams will eventually reach the detector. The two beams should fall on the same spot on the detector if their interference is to be measured. This is coincidence. The two light beams that are united at the detector should be as coincident and parallel as possible. This will allow large variations in intensity as the target moves. Figure 2-3 shows the incidence of two light beams on a target.

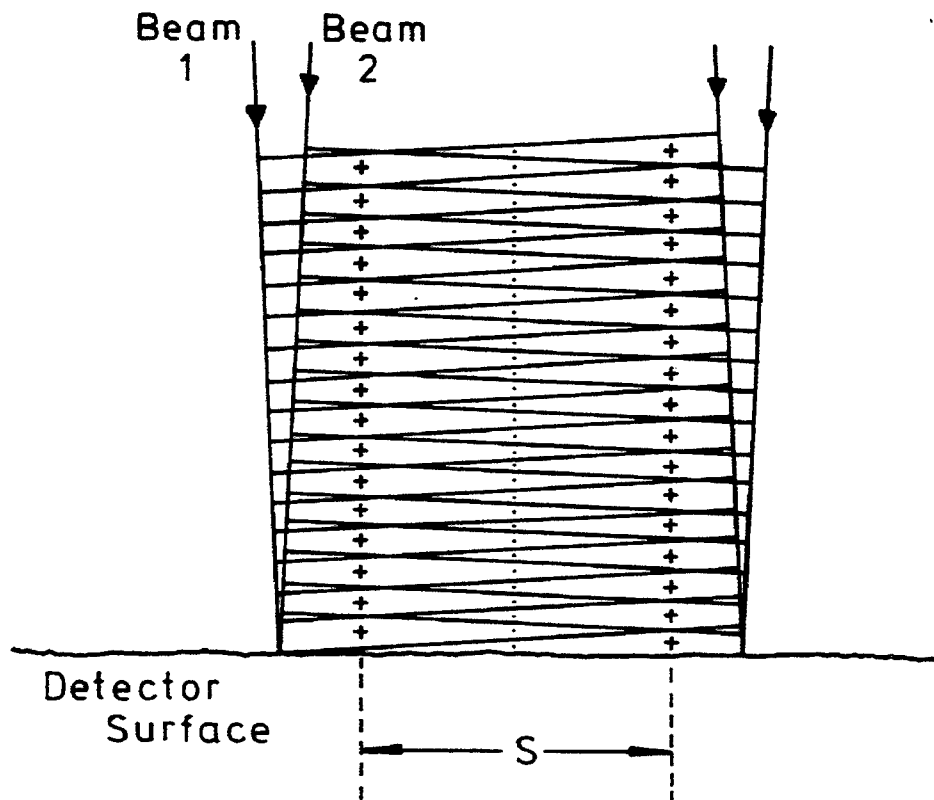


Figure 2-3 Angular Misalignment and Coherence (Scrubby, 1990)

If the beams have exactly the same wavelength but are out of parallel by a small angle β , then a constructive interference pattern will occur in the plane marked +++++. A destructive interference pattern occurs in the plane marked -----. The spacing of the fringes S , varies as the relative phase between the beams changes. The fringes move transversely across the detector. A given point on the detector will experience a fluctuation in intensity. If the fringe spacing is less than the beam diameter the fluctuations will tend to cancel each other. The fringe spacing can be defined as

$$S = \frac{\lambda}{2 \sin(\frac{1}{2}\beta)} \approx \frac{\lambda}{\beta}. \quad (2-11)$$

To achieve full efficiency η_h , called heterodyne efficiency, the beam width, D_b , should be less than half the fringe spacing S (Scruby, 1990). This means that the two beams should be parallel to within

$$\beta = \frac{\lambda}{2D_b}. \quad (2-12)$$

Thus a 10.6 μm wavelength two beams coincident on a detector, with a beam width of 1mm, should be parallel to within 5.3 milliradian. This should be achievable with the correct optics and alignment.

The process and components that enable us to achieve a coherent beam that can be frequency shifted and reflected off the target is described in the next part of the chapter.

B. CO₂ LASER THEORY

The Synrad G-48-1-28 CO₂ laser provides the backbone on the laser radar we constructed. The laser provides a coherent beam of 10.6 μm light and up to 10 watts of power when operating in the continuous wave (CW) mode. We will examine how the CO₂ laser transfers energy from electrical to coherent light with a wavelength of 10.6 μm .

1. The CO₂ Excitation Process

The first process in producing a coherent laser beam is the transfer of electrical energy to the pumping medium. In a CO₂ laser at least three gases are present: CO₂ provides the lasing medium, N₂ provides the pumping medium, while other inert gases such as He and Ne are present to provide electric discharge and thermal stability. Figure 2-4 shows the configuration inside the laser tube. An external DC power supply provides DC electrical power to the laser. Inside the laser an RF power supply converts the DC power into RF power. This RF drive consists of a power oscillator using a MOSFET to drive a push-pull amplifier consisting of two MOSFETs in saturation. The manufacturer

has matched the frequency of the RF power, about 45 MHz, to the resonant frequency of the plasma tube. An aluminum casing houses the RF drive assembly under the laser aluminum housing. RF power is fed into the laser housing to the top electrode. The bottom electrode is connected to the top electrode via a coil which phase shifts the RF power to the bottom electrode by 180°. Two grounding spacers further restrict the plasma and insulate the electrodes.

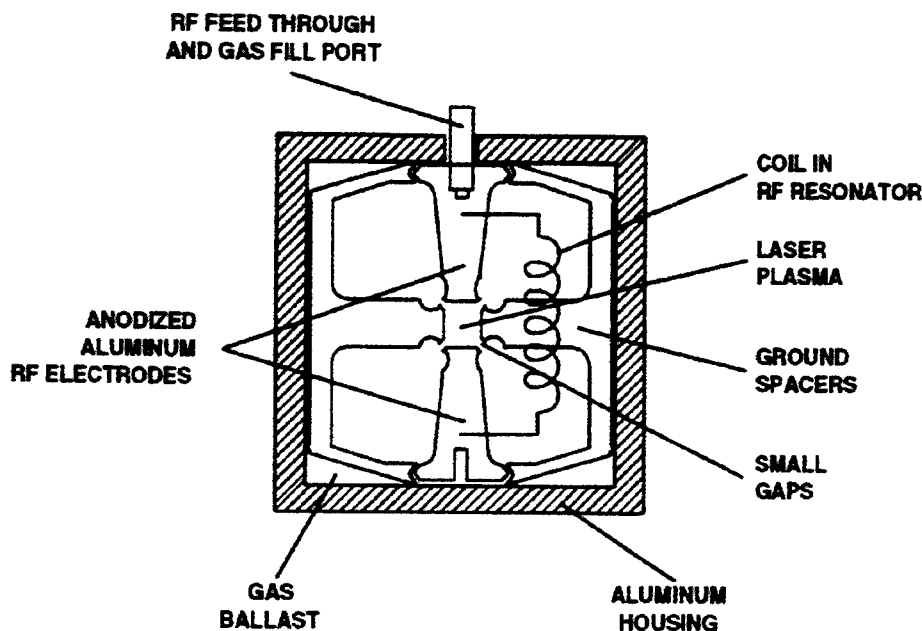
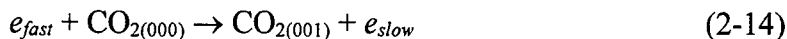


Figure 2-4 Synrad Laser Cross-Section (Synrad, 1996)

The RF driver delivers 1000 Volts peak to the electrodes. This sets up an oscillating electric field that transfers electrical power via three processes; electronic ionization, gas heating and vibration excitation to the plasma tube. Inside the tube a gaseous mixture of CO₂, N₂, He as well as other inert gases is subjected to this high voltage oscillating electric field. Electronic excitation and ionization occur freeing up electrons. This sets up and maintains the discharge. The electrical field also transfers power to the free electrons speeding them up. These fast light electrons collide with the more massive neutral atoms of the gas mixture. Collisions are both elastic and inelastic and enough occur to raise the average kinetic temperature of the gas mixture. The high speed electrons also collide with and transfer energy to CO₂ and N₂ molecules via an

inelastic processes. These collisions change the vibrational and rotational states of the CO₂ and N₂ molecules according to the following chemical equations:



Fast moving electrons, e_{fast} , collide with both N₂ and CO₂ molecules. These molecules start off in the vibrational ground state and are raised to a higher vibrational states by the collision, N₂ ($v=n \leq 8$) and CO₂ ($v=001$). These fast electrons can excite the N₂ molecules from the ground state into one of eight higher states. The CO₂ molecule starts off in the ground state, but has three vibrational modes.

Figure 2-5 shows the three modes for the CO₂ molecule; ν_1 -the symmetric stretching mode, ν_2 -the bending mode and ν_3 -the asymmetric stretching mode. Fast electrons can raise the CO₂ molecule's energy level in any one of these modes:

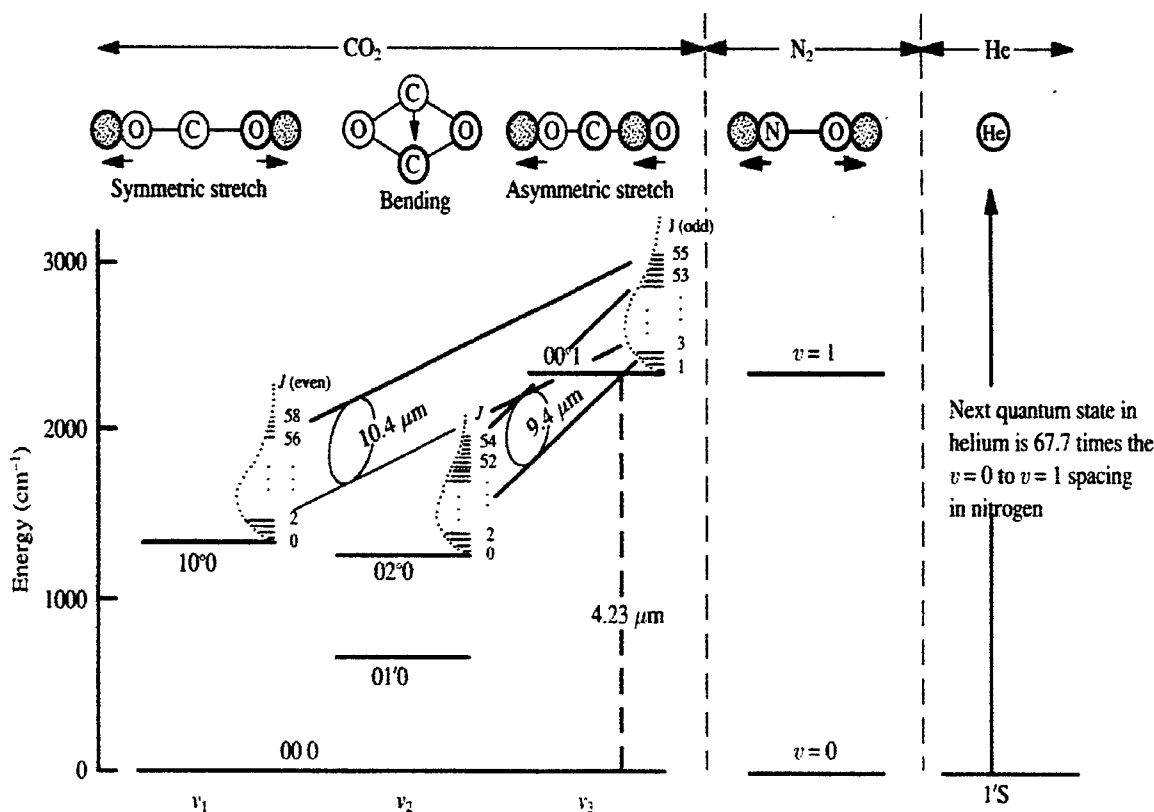


Figure 2-5 CO₂ Energy Level Diagram (Hawkes, 1995)

The N₂ molecule has only one vibrational mode. It also has the special properties of being a homonuclear diatomic molecule. It can not form an electric dipole and thus can not readily give off photons to drop to a lower energy state (Verdeyen, 1995). Thus N₂ is metastable in its higher energy levels. One of the only ways the N₂ molecule can drop to a lower energy level is by resonant energy transfer (Harney, 1996). When the energy levels of two different molecules are roughly the same, collisions between two molecules easily transfer energy during a collision. In this process N₂ has an energy level ($v = 1$) that is very close to the asymmetric stretching mode energy level (001) of CO₂. The metastable N₂ molecules in the $v=1$ energy level can now transfer their energy and drop to their ground state.

CO₂ molecules in the asymmetric stretching mode (001) can give off energy by the spontaneous emission of a photon of light and changing to the bending mode (020) or to the symmetric stretching mode (100). It is important to note that selection rules derived from quantum physics apply in determining what energy levels the CO₂ molecule can change to. Allowed vibrational-rotational transitions include:

$$\begin{aligned}\Delta v &= \pm 1 \\ \Delta J &= \pm 1, 0\end{aligned}\tag{2-18}$$

ΔJ represents the change in rotation energy levels. Rotational energy levels involve much smaller energies than the vibrational transitions seen in Figure 2-5 (Verdeyen, 1995). These selection rules define over 200 vibrational-transitions that allow transitions from 8 μ m to 18 μ m in wavelength. The 10.6 μ m lasing wavelength used in our laser comes from the 001 \rightarrow 100 vibrational transition. Figure 2-5 shows the wavelength emitted during this transition as 10.4 μ m. This is for a rotational transition for which $\Delta J = 0$. The difference between the 10.4 μ m shown and actual 10.6 μ m achieved involves the higher level rotational transitions.

Verdeyen has listed the transition probabilities for the primary transitions involved in the lasing process. Probabilities range from 0.34 to 0.33 sec⁻¹ for 10.4 μ m (001 \rightarrow 100) transitions and 0.20 to 0.19 sec⁻¹ for 9.4 μ m (001 \rightarrow 010) transitions. This means the radiative lifetimes (the inverse of the transition probabilities) range from 3 to 5 seconds. Thus spontaneous emission for these wavelengths do not have large enough losses to be

considered in the laser rate equations. The 4.2 μm transition has transition probabilities of approximately $2.0 \times 10^2 \text{ sec}^{-1}$. The resulting radiative lifetime for 4.2 μm is 5 milliseconds. The majority of the losses come from spontaneous 4.2 μm transitions. The energy exchange between colliding molecules has a much larger effect. We will not totally ignore spontaneous emission since it plays an important part in providing the "spark" to start the lasing process.

2. The Emission Process

Einstein described processes that related the absorption and emission of electromagnetic radiation from atoms and molecules. The famous Einstein coefficients describe the rates at which atoms and molecules spontaneously absorb and emit radiation as well as a process called stimulated emission.

Stimulated emission is critical to the function of the laser radar. It is the process in which an incoming photon will stimulate the excited CO_2 molecule to give off a photon and drop to a lower energy level. What's special about this process is that the stimulated photon has the same direction, frequency, phase and polarization as the inducing photon. Compare this to spontaneous emission where the molecules emit photons in a random uncontrollable fashion. The frequency will be the same; but the polarization, phase and direction are random. Spontaneous emission yields incoherent radiation while stimulated yields coherent light. Figure 2-6 shows (a) spontaneous emission, (b) stimulated absorption and (c) stimulated emission.

As the photons travel throughout the lasing medium they will encounter other CO_2 molecules in the excited state. These molecules are also stimulated into emission and a gain in the intensity results. The change in intensity I_ν over a distance z can be described by the equation

$$\frac{dI_\nu}{dz} = \left[A_{21} \frac{\lambda^2}{8\pi n^2} g(\nu) \right] \left[N_2 - \frac{g_2}{g_1} N_1 \right] I_\nu = \gamma(\nu) I_\nu, \quad (2-19)$$

where A_{21} is the spontaneous emission coefficient, λ is the wavelength of emitted radiation, N_1 is the number of CO_2 molecules energy level 1 per unit volume, N_2 is the

number of CO₂ molecules energy level 2 per unit volume, n equals $N_2 - N_1$, $g(\nu)$ equals the lineshape, g_1 equals the number ways that the CO₂ molecule can have energy level 1, g_2 equals the number ways that the CO₂ molecule can have energy level 2 and $\gamma(\nu)$ equals the gain coefficient.

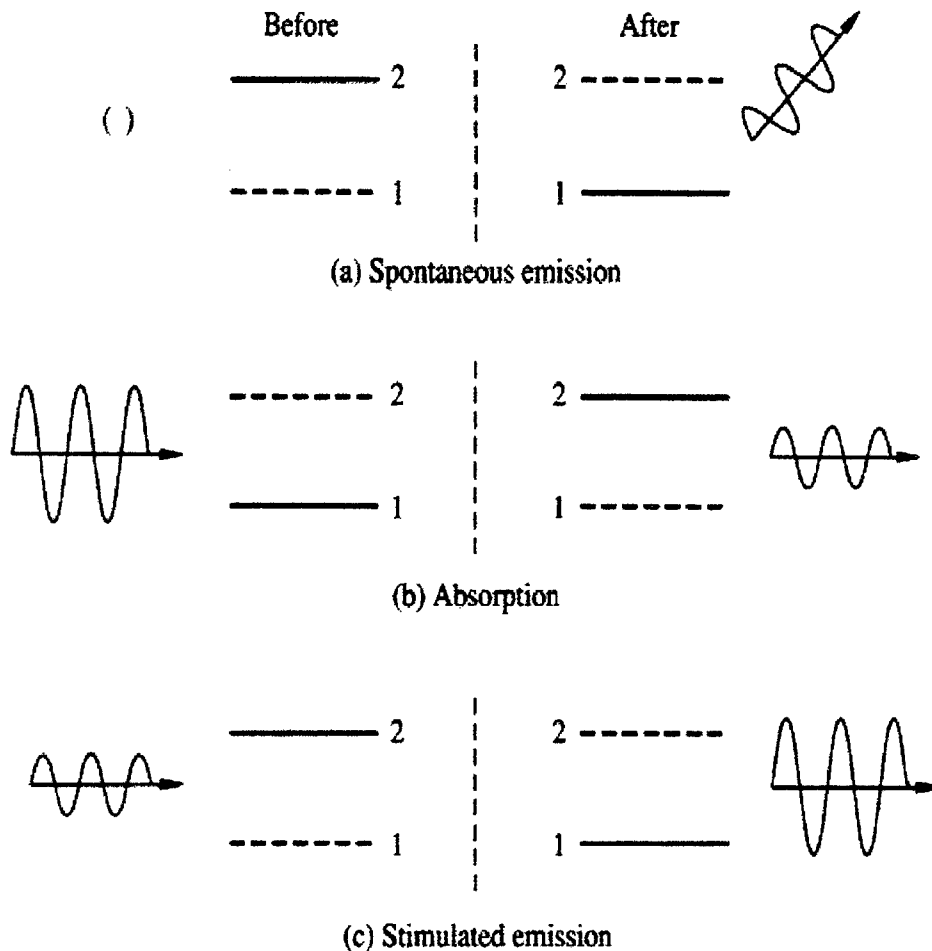


Figure 2-6 Effects of Radiation on an Atom (Verdeyen, 1995)

The importance of this equation comes from the terms in the second bracket. The terms in the left bracket are almost always positive. Therefore, if the right bracket is positive, gain will occur. If the bracket is negative attenuation will occur. Rearranging the right bracket yields

$$\frac{N_2}{N_1} \geq \frac{g_2}{g_1}. \quad (2-20)$$

This is the condition for laser gain, corresponding to population inversion requirement. Just to have gain is not enough to produce a useable laser. The desire is to achieve laser oscillation and amplify the forming beam to a useful level.

3. Feedback, Oscillation and Amplification of Laser Light

Anyone who has heard the annoying loud squeal from a microphone placed to close to a speaker has experienced the effects of feedback oscillation. In much the same way, a laser will use feedback to create an oscillator that is capable of amplifying the laser light. The CO₂ laser has a gain medium sandwiched in between two mirrors. Figure 2-7 shows a basic side view of the Synrad laser. Equation 2-19 describes the gain in beam strength as it travels the length of the gain medium.

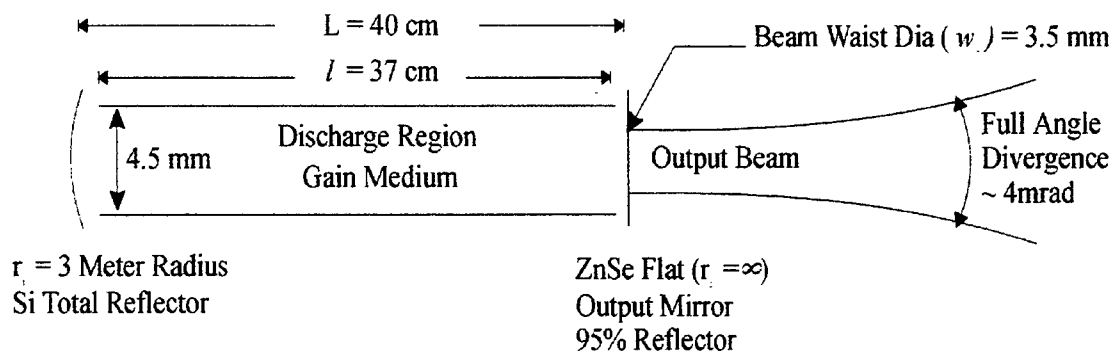


Figure 2-7 Laser Configuration

Verdeyen has derived the gain experienced in one pass through a distance of l in the gain medium:

$$G_0 = e^{\gamma l} \quad (2-21)$$

If the reflectance of the two mirrors involved (R_1 and R_2) are the only losses, then the threshold for oscillation becomes (Verdeyen, 1995):

$$R_1 R_2 e^{2\gamma l} \geq 1 \quad (2-22)$$

Admittedly, there are many other processes that will cause losses to occur as the beam travels through the medium; however, the fact remains that the gain must overcome the losses in the medium in order for the laser to break threshold and begin to oscillate and

amplify. Incident photons stimulate the CO₂ molecules. These molecules emit their photons and drop to lower energy levels. They must be “pumped up” fast enough or the gain will decrease below the threshold and lasing cease. Oscillation and amplification occur if the net gain per unit length is greater than the net loss per unit length. As amplification increases the rate at which CO₂ molecules drop down into the lower energy state also increases. Eventually, the gain will reach a saturation point where the pumping process can no longer keep up with the combined effects of lasing and losses and the laser will settle into steady state.

Laser designers need to configure mirrors so that resonance can occur. This means that as the beam reflects back and forth within the resonator cavity, it will eventually retrace itself before missing a mirror and being absorbed by the cavity walls. These configurations are called stable configurations. The following criteria can be used to determine if the lasing cavity is stable (Harney, 1996).

$$0 \leq g_1 g_2 \leq 1 \quad (2-23)$$

where

$$g_1 = 1 - L/r_1 \quad (2-24)$$

and

$$g_2 = 1 - L/r_2, \quad (2-25)$$

here L equals cavity length, r_1 equals radius of curvature for mirror 1, r_2 equals radius of curvature for mirror 2.

For the case of our Synrad laser, the first mirror had a radius of 3 meters and the second mirror was flat. This resulted in a stable configuration with $g_1 g_2 = 0.866$. The laser is thus a stable oscillator that amplifies coherent light. The next section shows how the frequency of the laser can be selected.

4. Line shape, Cavity Modes and Lasing Threshold.

Lineshape also plays a part in getting the laser to lase at the proper frequency. Despite the fact that the molecules have discrete energy levels, these levels are not exactly the same in each molecule. For a given vibrational and rotational energy level small

variations in energy exist between different molecules. A number of factors contribute to this effect; the uncertainty principle, isotope effects, Doppler shift and gas pressure are just a few. Their resulting effect is to "broaden" the spectral emission line from a precise frequency to a range of frequencies $\Delta\nu$. This effect is called line shape $g(\nu)$. We will use the definition that $g(\nu)d\nu$ is the probability that an emitted photon will have a frequency between ν and $\nu + d\nu$. The sum over all possible frequencies will total 1 with the highest probability centered on the original frequency. The line shape directly effects the gain coefficient $\gamma(\nu)$. The resulting shape of the gain coefficient resembles a Lorentzian function as shown in Figure 2-8.

In order to set up oscillation, designers will place mirrors at a specific distance to set up a standing wave in a resonant cavity. These standing waves will satisfy the following condition (Wilson, 1989)

$$p \frac{\lambda}{2} = L, \quad (2-26)$$

where p equals an integer, L equals the optical path length and λ equals the lasing wavelength.

Cavity mode frequency separation can be found for the laser cavity by converting the wavelength to a frequency and setting $\Delta p = 1$:

$$\Delta\nu = \frac{c}{2L}. \quad (2-27)$$

For the Synrad laser $\Delta\nu = 375$ MHz. These are the frequencies allowed by the physical layout of the laser cavity. Figure 2-8 shows how the broadened transitions combine with the cavity modes to shape the possible frequency outputs of the laser. The dashed lasing threshold line shows how strong the resulting axial modes have to be in order to oscillate. The stronger the intensity, I of an axial mode the faster it will amplify. This draws down the available upper level molecules at a faster and faster rate. It becomes a case of only the strongest axial mode surviving as it starves the other axial modes below threshold. In the Synrad laser used for our studies, the lasing cavity was designed to have a center lasing wavelength of $10.6 \mu\text{m}$ or a frequency of 28.3×10^{12} Hz.

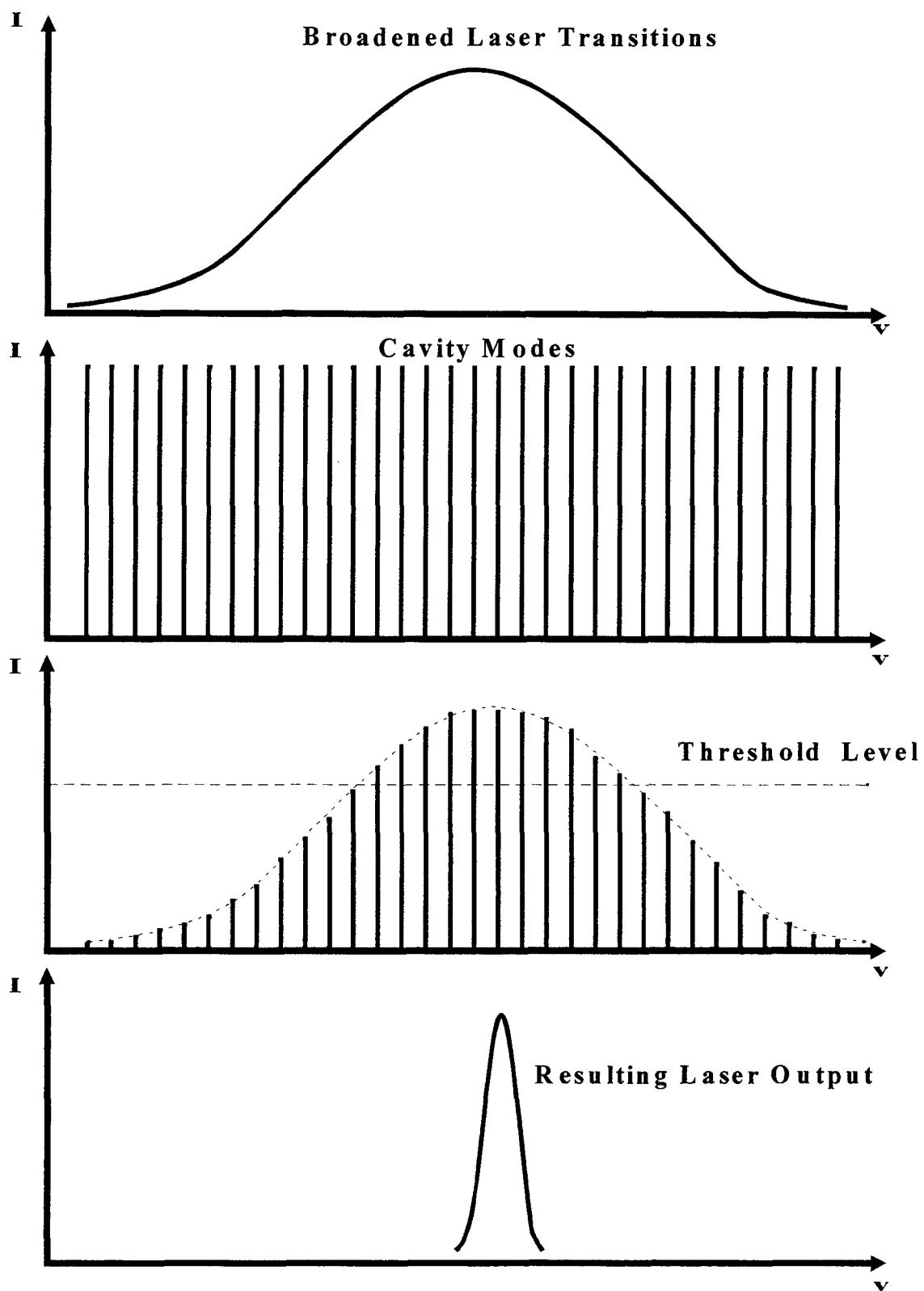


Figure 2-8 Laser Frequency Control

A final word on the lasing frequency; the frequency can shift as the laser cavity heats up and thermally expands. The expanding cavity length, L decreases the frequency separation and changes the lasing frequency. For the Synrad laser this thermal expansion can cause a wavelength shift from $10.57\text{ }\mu\text{m}$ to $10.63\text{ }\mu\text{m}$.

5. Gaussian Beams and Hermite-Gaussian Mode Patterns

There are many paths inside the laser cavity that will lead to the beam repeating itself in a standing wave and thereby amplifying itself. The beam does not have a uniform intensity across its diameter as it exits the laser cavity. Its intensity is stronger in the center of the beam pattern and tapers off towards the edges of the beam. The intensity pattern can have many different symmetrical patterns. These are the Hermite-Gaussian modes. A detailed description of how these patterns are formed is contained in Anthony E. Siegman's book on lasers. (Siegman, 1986) Resonant modes of replicating paths that form off the center axis of the laser cavity will have components of their electromagnetic fields that are transverse to the direction of propagation. The simplest transverse electromagnetic mode has the intensity profile the shape of a Gaussian. This is the Hermite-Gaussian Mode 0,0 shown in Figure 2-9 (Siegman, 1986). Other Hermite-Gaussian modes exist and are more complicated. The more complicated modes cover a larger area. They are less desirable in most laser applications due to their complex intensity patterns. Laser designers can control these less desirable modes by controlling the size of the laser cavity and exit aperture. Shrinking these sizes allows all of the lower level modes to form and only a small percentage of the higher modes to lase. The Synrad laser has a mode purity for the lowest mode (0,0) of 98%.

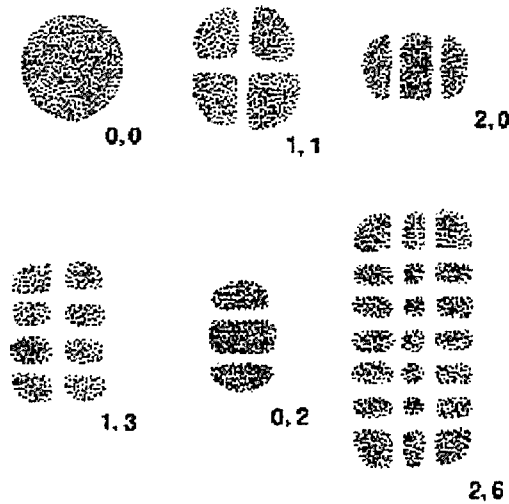


Figure 2-9 Hermite-Gaussian Modes (Siegman, 1986)

The laser beam is not a perfectly collimated beam. Gaussian optics describe how the beam will diverge and grow in diameter as it travels away from the laser. The diameter, or spot size w , is therefore a function of the distance z traveled. The relationship between the spot size and distance traveled is

$$w^2(z) = w_0^2 [1 + (z/z_0)^2], \quad (2-28)$$

here w_0 equals the beam waist radius and z_0 equals the characteristic length parameter of a Gaussian beam.

The beam waist radius is the minimum radius of the laser beam. Synrad engineers designed their laser to have w_0 at the exit aperture. This makes it easy to measure the beam divergence. The full angle divergence is four mrad for the Synrad laser. The laser beam is now described to the point where we can understand how DC power has been converted into coherent light with a 10.6 μm wavelength and a known intensity profile and divergence. A final question of laser efficiency will reveal how much power out are we getting for the DC power applied.

6. Laser Efficiency.

CO₂ lasers are capable of achieving some of the highest efficiencies possible. We measured the power applied to the laser and measured the laser beam output power to calculate the laser efficiency for various input voltages. Figure 2-10 shows the laser

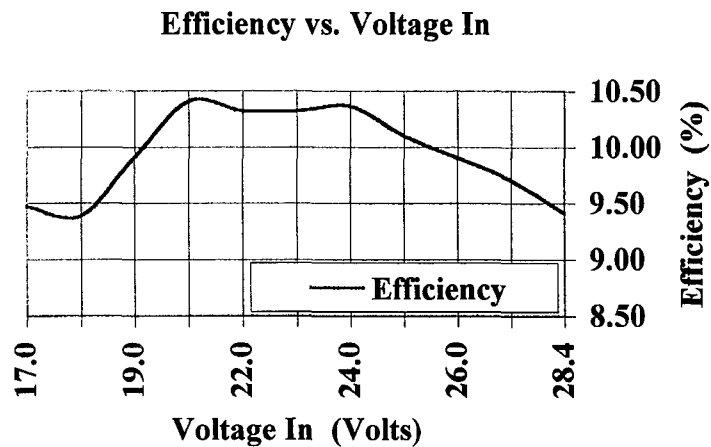


Figure 2-10 Synrad Laser Efficiency

efficiency. The Synrad laser achieves maximum efficiency in a range from 20 to 24 Volts. Figure 2-11 shows the power output the Synrad laser can achieve for a given voltage input. The most efficient ranges listed above had output powers of 10.6 Watts and 12.60 Watts respectively. These charts will enable us to more accurately control the laser output power.

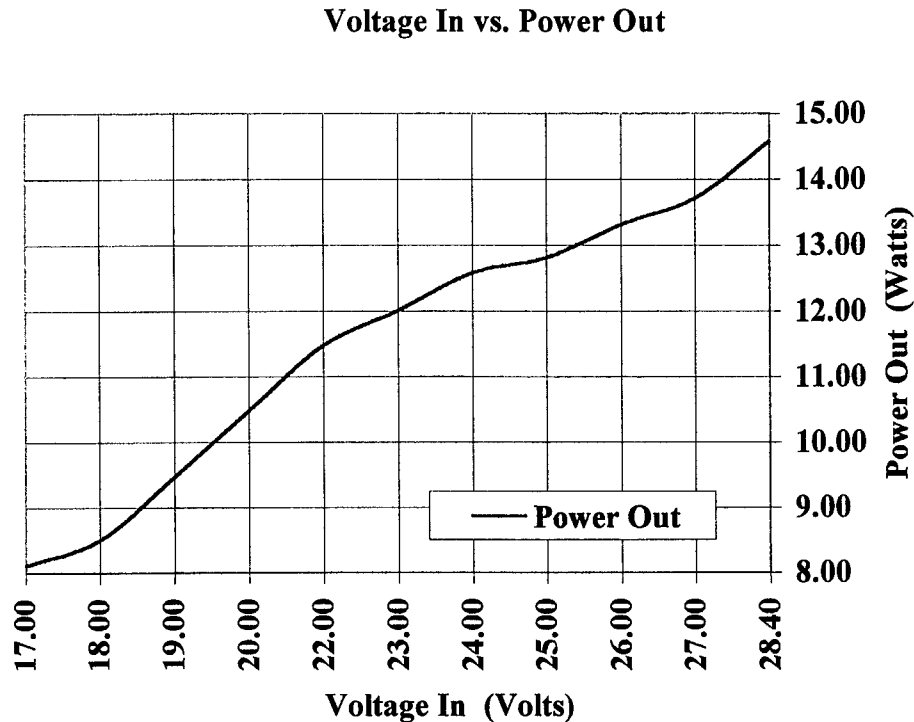


Figure 2-11 Synrad Laser Power Output

C. LENSES AND BEAM SPLITTERS

As the laser beam travels away from the laser, it will run through a series of beam splitters that divide and then recombine the beam. Lens will expand and collimate the beam as well as focus it onto detectors. Special materials that are transparent to $10.6\text{ }\mu\text{m}$ wavelength light are needed to create these lenses and beam splitters. Together these lenses and beam splitters allow us to set up heterodyne configuration. This section will cover the basic theory behind the lens and beam splitters used in our laser radar.

1. Lenses

Light traveling through a material can undergo an attenuation of its intensity as it travels through the material. This attenuation is wavelength and material dependent.

Unfortunately, most glass is not transparent at the 10.6 μm wavelength. Another material must be used to create lenses to expand and focus the laser light from our laser. Zinc selenide's properties make it transparent to light at 10.6 μm and therefore a good lens material. Lens designers can use the lens maker's equation to calculate the focal length, f of a lens.

$$\frac{1}{f} = (n-1)\left(\frac{1}{r_1} - \frac{1}{r_2}\right) \quad (2-29)$$

Figure 2-12 shows how the lens shapes the beam of light. Using ray tracing methods, when the light hits the first lens, r_1 , it bends as it encounters a change in the

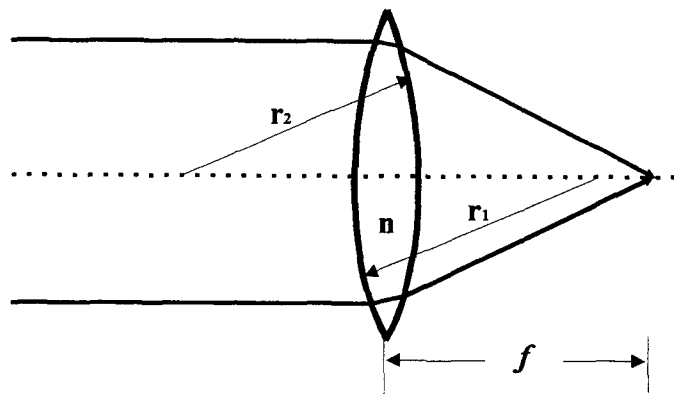


Figure 2-12 Lens Optics

refractive index, n . When the light exits the lens it bends again as it undergoes another sudden change in the refractive index. The focal length of the lens is where the two rays come together to form an image.

Lenses have many different shapes and sizes. Two of the most common (and the cheapest to fabricate) are the plano-concave and plano-convex lens. These lenses have one flat surface and one curved surface. This makes it easier to fabricate the lens. The lens maker equation now becomes

$$\frac{1}{f} = \frac{n-1}{r_1} \quad (2-30)$$

Typical focal lengths used to construct the laser radar include; 254mm, 150mm, 25mm and -50mm. Figure 2-13 shows the typical lens set-ups used in the laser radar.

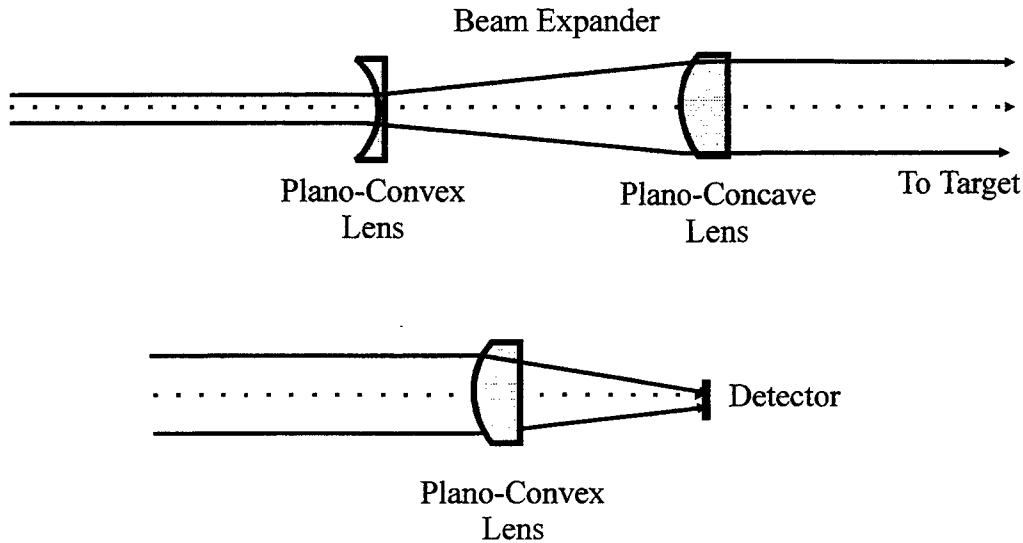


Figure 2-13 Lenses

2. Beam Splitters

Light can also reflect off the surface of a material. This is due to the sudden change in the index of refraction, n , that exists between the boundaries of the material along the laser beam's path. Laws that describe the reflection, refraction and transmission, are covered in all elementary books on optics (Hecht, 1987). When light hits the surface of the material, a fraction of the beam is reflected and the remainder of the beam will travel through the material. The total intensity reflected plus the total intensity transmitted must add up to the total intensity striking the material. Figure 2-14a shows this pictorially.

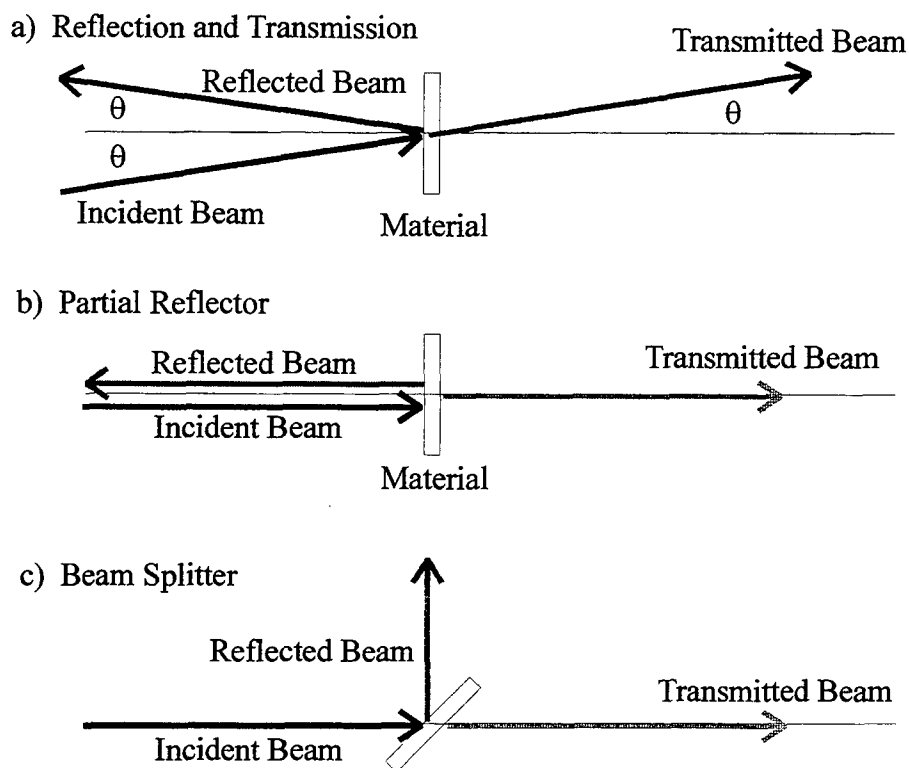


Figure 2-14 Beam Splitters And Partial Reflectors

Figure 2-14b shows the material used as a partial reflector. Designers use this set up to attenuate the light beam by a certain known percentage. Figure 2-14c is the set up for a beam splitter. In this configuration, the material is placed at a 45 degree angle to the incident beam. The beam then splits into two parts whose total intensity is equal to that of the incident beam.

Polarization of the laser beam also effects the beam splitter's reflection. Light emitted from the laser is vertically polarized. This corresponds to S-polarization. The manufacturer can measure the amount of reflection the beam splitter can deliver for both S and P polarizations. These values are measured when the lenses are produced and are provided with the lenses.

Beam splitter manufacturers will often design a slight wedge angle into their beam splitters to eliminate any interference effects. As light exits the material it reflects again back in the same direction as the reflected beam. If the two beams overlap interference

can result. Usually about 6 to 10 arc seconds of wedge angle are enough to eliminate these interference effects.

D. ACOUSTO-OPTIC MODULATION

The heterodyne configuration for the laser radar uses an acousto-optic modulator to shift the frequency of the laser light used in the laser radar. This section will describe the principles behind the acousto-optic effect. When a medium is subjected to compressive and rarefractive pressure waves, its refractive index, n_m will change as a result of the mechanical strain (Wilson, 1989). Acoustic pressure waves can thus generate changes in the medium's refractive index. The amount of change in the refractive index is proportional to the square root of the total acoustic power applied to the medium. (Wilson, 1989). High acoustic pressures will generate a higher refractive index while lower acoustic pressure will generate a lower refractive index.

If the medium is transparent to the incident light, the light beam encounters the effects of the changing refractive index. The areas of low pressure and thus low refractive index will allow the light to pass through faster. High pressure areas will slow the incident light down. If the incident light passes through the medium in a direction normal to the acoustic waves, a modulated optical wave front will result. A standing acoustic wave in the medium wave will create a diffraction grating with the spacing of the acoustic wavelength, Λ .

There are two types of modulators. Thin mediums are designed to modulate the amplitude of the incident beam. Thicker mediums can be set up to modulate the frequency of the incident light beam. Since we are interested in modulating the frequency of our laser beam, we will concentrate on the thicker medium case called the Bragg regime.

In the Bragg regime the diffraction is so complete that the acoustic field acts like planes of "traveling mirrors." Figure 2-15 shows this configuration. These traveling mirrors reflect the incident light. Careful design of the acousto-optic modulator setup will require that light reflecting off of successive traveling mirrors arrive in phase at the new reflected wavefront. Therefore, the path differences between the successive reflections off

the traveling mirrors must be integer number of wavelengths. In order to achieve this condition the light beam must come in at a specific angle. This angle is called the Bragg angle, θ_B and is given by

$$\theta_B = \sin^{-1}\left(\frac{m\lambda}{2\Lambda}\right). \quad (2-31)$$

The order of diffraction, m , is taken to be equal to 1 in most cases. Incident light that has an incident angle, θ_i , equal to θ_B reflects with its wavefront intact. Placing an

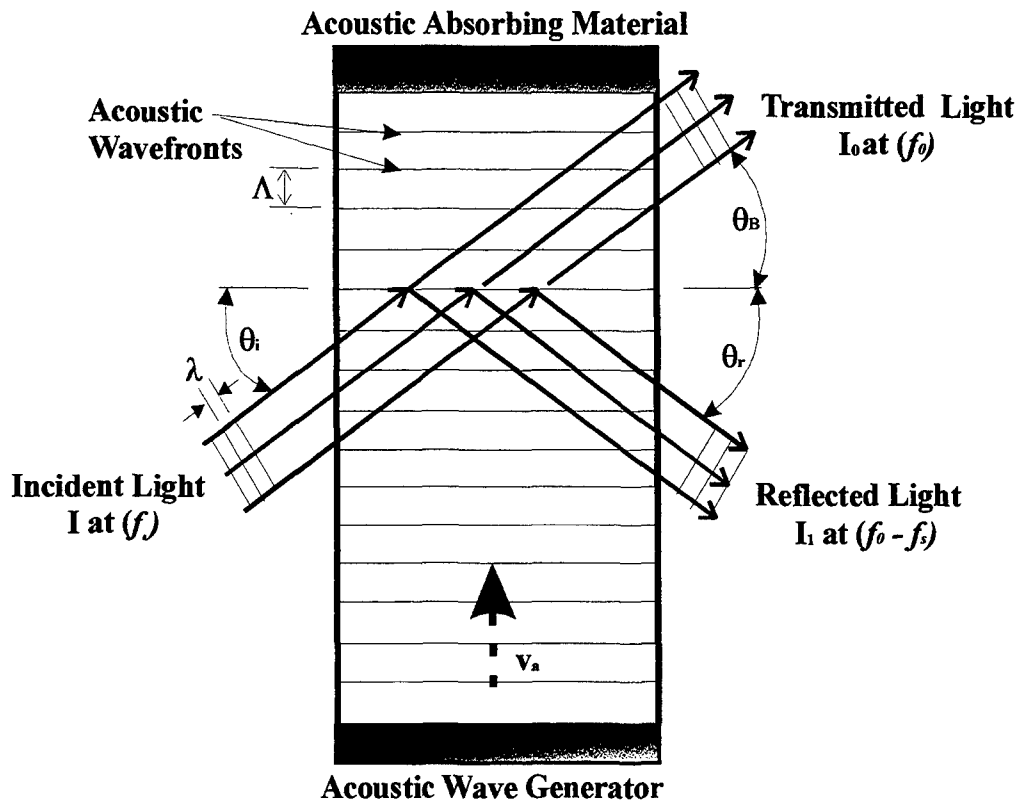


Figure 2-15 Acousto-Optic Modulator

acoustic dampener at the far end of the modulator allows acoustic waves to travel through the medium creating “traveling” diffraction planes. Incident light reflected off of these traveling diffraction planes will be Doppler shifted. The amount of Doppler shift is:

$$\Delta \nu = \frac{\pm 2n_m v_a \sin \theta_B}{\lambda} \quad (2-32)$$

Combining equations 2-29 and 2-30 result in the modulator shift of $\pm v_a/\Lambda$. This is just the modulator shift frequency, $\pm f_s$, or the acoustic wave frequency. The \pm symbol means the frequency can be up shifted or down shifted depending on the orientation of the acousto-optic modulator or the direction of travel for the acoustic waves. If the acoustic waves travel into the incident light waves, the light frequency will be shifted up by f_s . If the acoustic waves travel with the incident light they will downshift the incident light frequency by f_s . We can use this shift in frequency as our shift frequency in our laser radar.

The modulator used in our experiment contains a high grade single Germanium crystal that is transparent at 10.6 μm . It has a thin anti-reflection coating also designed to operate at 10.6 μm . Piezoelectric generators driven by an RF power source provide the acoustic signal at a frequency of 30 MHz. The intensity of the reflected light, I_1 is dependent on the diffraction efficiency. The diffraction efficiency for the first order, $m = 1$, depends on the RF power. Table 2-1 shows how the diffraction efficiency for our

RF Power (Watts)	Diffraction Efficiency ($m = 1$)
5.0	29.3%
10.0	48.1%
15.0	67.0%
20.0	74.9%
25.0	80.1%
30.0	84.9%

Table 2-1 Acousto-Optic Modulator Efficiency (IntraAction Corp., 1996)

acousto-optic modulator varies with RF power applied. The maximum power achieved a diffraction efficiency of almost 85%. For an incident laser beam of 10 Watts, 8.5 Watts would be reflected and frequency shifted by 30 MHz. The remaining fraction of intensity

would be found in the transmitted beam. The transmitted beam remains at the same frequency.

E. DETECTORS

The detector converts the returning laser light into an electrical signal. The returning signal is first collected by a series of lenses and focused onto the detector. Our laser radar used a photoconductive type detector. The detector is a semiconductor device that uses a mercury-cadmium-telluride (HgCdTe) alloy to create a precise energy band gap, E_g , between the valence and conduction bands of the semiconductor. Band gap energies can range from zero to 1.6 eV (Wilson, 1989). An incident photon can raise an electron into conduction band of the semiconductor if it has enough energy. Since the energy of the photon is related to its wavelength, the wavelength of the photon determines if the photon will cause an electron to jump up into the conduction band

$$\lambda_c = \frac{hc}{E_g}, \quad (2-33)$$

where h is Planck's constant and c equals the speed of light. As long as $\lambda \leq \lambda_c$, the cut off wavelength, the electron makes the jump.

Absorption of the right wavelength of an incident photon will raise an electron into the conduction band and thereby increase the conductivity of the semiconductor. This means the resistance of the material will go down as more and more photons are absorbed by the semiconductor. A simple way to measure the effectiveness of the semiconductor detector is the photoconductive gain, G . The gain equals the flow rate (electrons/second) divided by the rate of electron-hole pair generation. The photoconductive gain is proportional to a bias voltage applied and inversely proportional to the detector area. Care must be taken not to increase the bias voltage too high or the semiconductor will become saturated.

As electrons are raised an electron-hole pair is created. In equilibrium; the rate of formation of electron-holes will equal their recombination rate. One cause of detector noise comes from fluctuations in the generation and recombination rates. Thermal energy

can also create electron-hole pairs. Thermal generation is a primary concern of designers trying to control noise in the detector. This thermally generated noise is proportional to $\exp(E_g/2kT)$. T is the absolute temperature and k is Boltzman's constant. As the semiconductor temperature goes down, the noise also goes down. Many detectors are cooled to reduce their noise since noise limits the detector's ability to detect small signals. The noise equivalent power, NEP is a measure of how easily a detector can distinguish a small signal from the noise within the detector. Many designers however will use a parameter called the specific detectivity

$$D^* = \frac{(A \Delta f)^{\frac{1}{2}}}{P} \left(\frac{V_s}{V_n} \right) \text{ (cmHz}^{1/2}\text{/W)}. \quad (2-34)$$

The detector area is represented by A (cm^2), Δf equals the electrical bandwidth (Hz), P equals the incident power (Watts) and V_s/V_n equals the rms. signal-to-noise ratio.

This parameter characterizes the signal-to-noise ratio in a 1 Hz bandwidth per unit rms. incident radiant power per square root of detector area (Schlessinger, 1995). If current is measured, then I_s/I_n is used instead of V_s/V_n . For the detectors available for our laser radar D^* ranged from 6.7×10^6 (($\text{cm}\sqrt{\text{Hz}}\text{)/W}$) for the room temperature HgCdTe detector to $\geq 5 \times 10^{10}$ (($\text{cm}\sqrt{\text{Hz}}\text{)/W}$) for the liquid nitrogen cooled HgCdTe detector in the $10.6 \mu\text{m}$ range.

Responsivity R , is another measure of detector performance. Responsivity measures the output of the detector (usually in Volts or Amps) versus the incident power of the light at the peak wavelength. Typical ranges of responsivity for the detectors available for our laser radar are from 100 (mV/W) for the room temperature detector to 5,280 (V/W) for the liquid nitrogen cooled detector. The typical configuration for the detector is shown in Figure 2-16.

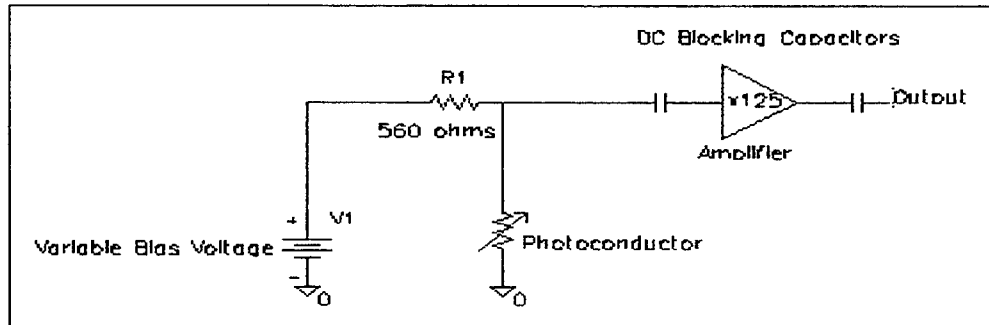


Figure 2-16 Detector Circuit Layout

Carrier to Noise Ratios (CNR) are often used to determine just how much incoming signal is needed to be distinguishable from the noise in the detector. For photoconductive detectors the current is used to define the CNR.

$$\text{CNR} = \frac{i_{\text{signal}}^2}{\sum i_{\text{noise}}^2} \quad (2-35)$$

There are a multitude of different noises that can have an effect on the SNR. These noises include shot noise, background noise, dark noise and the thermal noise already mentioned. Converting to power

$$\text{CNR} = \frac{\eta_D P_{\text{signal}}^2}{\sum K P_{\text{noise}}} \quad (2-36)$$

The detector's quantum efficiency η_D , represents the detector's ability to convert photons into current. The constant K , shown is a conversion constant that must be applied to convert the various noises into power terms. The heterodyne or coherent process combines the reference beam with the returning beam. The reference beam is often called the local oscillator.

The resulting CNR is

$$\text{CNR} = \frac{\eta_D P_{LO} P_{\text{signal}}}{hfB(P_{LO}) + \sum KP_{\text{noise}}} \quad (2-37)$$

The local oscillator acts like a noise term. If the local oscillator is strong enough, it will dominate the other noise terms. This simplifies the SNR relation and is a direct benefit of heterodyne process. The new CNR for a heterodyne configuration can be written as (Jelalian, 1992)

$$\text{CNR} = \frac{\eta_D P_{\text{signal}}}{hfB}, \quad (2-38)$$

where h equals Planck's constant, f equals the frequency of light used and B equals the electronic bandwidth.

For our configuration; the electronic bandwidth is the bandwidth established by the electrical filters used to select the vibrational frequency range.

F. LASER RADAR EQUATIONS

Radar equations have been developed for all types and classes of radar. Most radar equations expand upon the CNR of the detector. They include the effects of components as well as the detector. Additionally, fluctuations that effect the light beam as it travels to the target, reflects off the target and returns to the detector may be considered noise. In most cases these fluctuations give us no useful information. These effects include atmospheric turbulence, target scintillation of the beam and atmospheric attenuation of the beam to name a few. Additionally, components making up the laser radar effect the power of the outgoing and returning light signal. All of these effects can be added to the detector CNR equation to describe a CNR for the system.

For a laser radar the CNR is defined as (Harney, 1993)

$$\text{CNR} = \frac{\eta_D \epsilon_T \epsilon_R P_T e^{-2\alpha R}}{hfB} \left(\frac{\rho w_0^2}{R^2} \right) \left[1 - e^{\frac{-4\pi w_0^2 R^2}{\lambda^2 R^2}} \right], \quad (2-39)$$

where η_D equals the detector quantum efficiency, $\epsilon_T(\epsilon_R)$ equals the transmit (receive) path optics transmission efficiencies, w_0 equals the Gaussian spot size at the transmitting

aperture of the laser radar, α equals the atmospheric attenuation coefficient, ρ equals the target reflectivity, r_T equals the target radius, λ equals the wavelength of light used, R equals the range to the target, f equals the frequency of light used, h equals Plank's constant and B equals the electronic bandwidth. This equation assumes the target is a diffuse circular disk with a radius r_T at a distance R from the laser radar.

This equation can be simplified if two separate conditions are considered: For short range targets (the target is larger than the laser spot size at the range R)

$$\text{CNR} = \frac{\eta_D \epsilon_T \epsilon_R P_T e^{-2\alpha R}}{hfB} \left(\frac{\rho w_0^2}{R^2} \right). \quad (2-40)$$

For long range targets (the target is smaller than the laser spot size at range R)

$$\text{CNR} = \frac{\eta_D \epsilon_T \epsilon_R P_T e^{-2\alpha R}}{hfB} \left(\frac{4\pi^2 \rho r_T^2 w_0^4}{\lambda^2 R^4} \right). \quad (2-41)$$

These are the radar equations for heterodyne laser radar configuration. The short range equation (resolved target) yields a CNR proportional to $1/R^2$. The long range equation (unresolved targets) yields a CNR proportional to $1/R^4$. These results are similar to the traditional radar equation's reliance upon range. Laser radar designs will match the optics of the system to the Gaussian spot size w_0 . The transmitting optics diameter D , will be sized so that the majority of the intensity of the Gaussian beam profile will pass through the lens configuration. For mathematical convenience we will assume $D = 2\sqrt{2}w_0$ (Harney, 1993).

The theoretical range of our laser radar can now be calculated. Assuming the use for our laser radar would be to identify ground vehicles and using components (beam splitters, lenses, lasers, detectors, etc.) that were available in the laboratory, calculations were made using the configuration shown in Figure 2-1. Figure 2-17 shows the CNR for a given range. We used the resolved target equation since at this range the laser spot diameter would be smaller than any vehicle. The quantum efficiency was assumed to be 0.5 and the optical system could transmit and receive at 21% and 52% efficiency with 25mm optical lens. The maximum power the laser was taken at 13 Watts at a $10.6 \mu\text{m}$ wavelength. The electronic bandwidth was 10 MHz due to the inexpensive filters available. The atmospheric attenuation coefficient was taken to be about 0.9

corresponding to a 10 km visibility. The target reflectivity was assumed to be about 0.1. Which is close to what a dirty flat black painted target would reflect (Jelalian, 1992). Most systems will have a required CNR. Above this required CNR value detection is highly probable. For most radar systems 15dB is a common value of CNR required. A CNR of 15dB would allow detection of vibrations out to 6.5 km for our system.

CNR vs Range for Resolved Targets

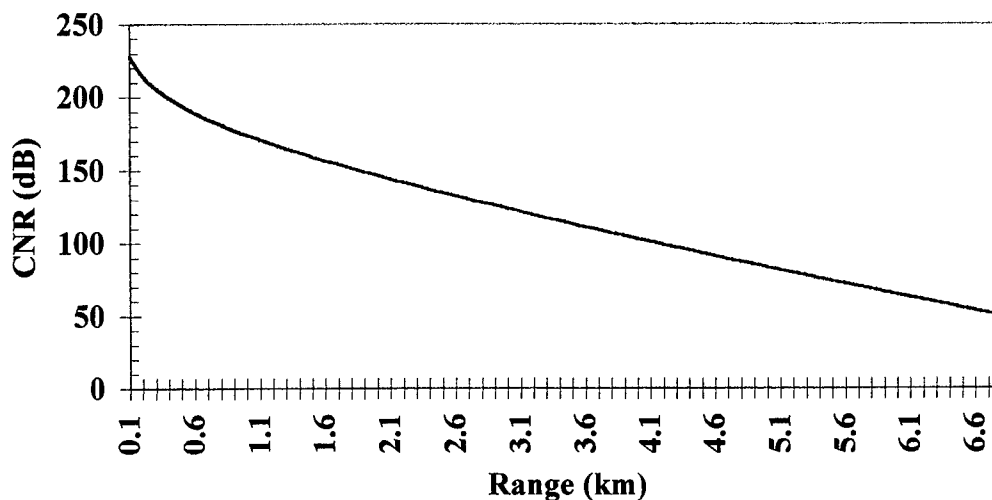


Figure 2-17 CNR Vs. Range (km)

The most critical factor that can be readily changed is the electrical bandwidth. Currently 10 MHz band pass filters are available. If a band pass filter of 100 kHz were used; the maximum range of the system would jump to 8.7 km. This would provide the cheapest way to improve the range.

III. EXPERIMENTAL SET UP

This chapter covers the setup of the laboratory, laser radar and measuring equipment. We set up the laser radar in the laboratory room that required certification to Class IV standards by the Naval Postgraduate School Radiation Safety Officer. Once the Radiation Safety Officer certified the laboratory to handle Class IV lasers, we were able to construct and test the setup of the laser radar.

A. SAFETY

The Synrad laser used in our laser radar is a category IV laser. Its infrared wavelength combined with its power output require special procedures and safety equipment to operate the laser. This was critical since the amount of adjustments and alignments required the laser radar to be in an open setup. This open configuration allowed full access to the lenses and laser but it also allowed for accidental exposure to the harmful laser radiation. We conducted a risk assessment of the experiment (shown in Table 3-1) to identify the hazards and mitigating steps to reduce the hazard potential.

Source of Hazard	Hazardous Effect	Mitigating Steps
Laser Beam & Reflections	<ul style="list-style-type: none">•Eye Damage•Skin Damage	<ul style="list-style-type: none">• Wear Certified CO₂ Goggles• Wear Protective Clothing (Long sleeve shirts, etc.)
Power Supplies	<ul style="list-style-type: none">•Electrocution•Shock Induced Accidents	<ul style="list-style-type: none">• No modification of commercial power supplies.• Keep the work area clear of unnecessary tools
Experimental Procedures & Set-Ups	<ul style="list-style-type: none">•Falls, Tripping over cables and in the dark	<ul style="list-style-type: none">• Keeping area surrounding the laser clear of cables and equipment
Target Material (intended or unintended)	<ul style="list-style-type: none">•Ignition•Toxic Vapors	<ul style="list-style-type: none">• Use of Beam Stops (Fire bricks)• Fire Extinguisher

Table 3-1 Experimental Hazards

We used these steps inside the laboratory. We modified the room to ensure no hazards existed outside of the laboratory.

1. Class IV Laser Room

The laboratory room was located in the basement of Spanagel Hall (Room 018). The windows in the room were clear glass. We covered the windows with heavy felt and black cloth. Regular glass would normally absorb laser radiation at $10.6\mu\text{m}$ wavelength at 10 Watts. The felt and cloth allowed us to darken the room to measure IR light and for future use of higher powered lasers.

We installed an interlock on the entrance to the laboratory. The interlock acts to shut off the laser power supply the instant the laboratory door inadvertently opened. Figure 3-1 shows the design used to construct the interlock. A transformer inside the interlock converted power from a 110 Volt AC source into 24 Volts AC. A line carries this voltage to the laboratory door through a relay. If anyone opens the door, the

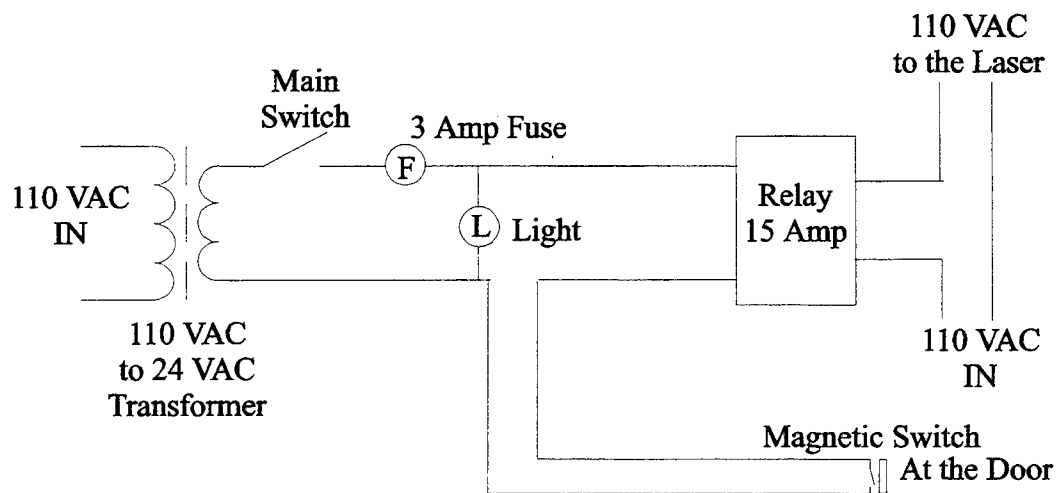


Figure 3-1 Interlock Design

interlock circuit opens and the relay disconnects the power to the laser. When the laboratory door is closed, the circuit is closed and the laser receives power. The main

switch provides a way to cut the power to the laser in the event of an emergency without opening the door. This provides a fifth way to shut off the laser if an emergency occurs. The different methods to shut down the laser include: shutting the lens to the laser, turning the laser key switch located on the back of the laser body, turning off the laser control voltage and turning off the main power supply to the laser. Any one of these methods of turning off the laser was within easy reach from the operating area.

2. Laser Safety Distances

The Synrad laser has a maximum measured continuous wave power output of approximately 15 Watts. The output diameter of the beam is 3.5 mm at the laser exit aperture (Synrad, 1996). The resulting beam intensity of 311.8 W/cm^2 is several orders of magnitude greater than the maximum permissible exposure (MPE) of 0.1 W/cm^2 for direct viewing of $10.6 \text{ }\mu\text{m}$ wavelength laser light (ANSI Z136.1, 1993). The maximum exposure time to the MPE is 10 seconds. The MPE for skin exposure is the same. The nominal ocular hazard distance R_{NOHD} , is approximately 50 meters. The R_{NOHD} is the range at which eye or skin protection is no longer needed. The laboratory experimental area is less than 10 meters. Therefore, we wore protective eye wear and clothing during all experiments.

The nominal hazard zone range R_{NHZ} , was calculated for the available protective eye wear. The R_{NHZ} is the minimum radius away from a diffuse reflecting surface that an observer should be. Laser goggles designed for CO_2 lasers were available in laboratory. These goggles had an optical density rating of five. The nominal hazard zone for an observer using these goggles would be zero meters. Direct viewing of the laser light would seemingly require a set of safety goggles with an optical density of approximately 3.5. However, a beam intensity of 300 W/cm^2 would quickly (seconds) burn a hole through the goggles. The protective eye wear in the laboratory offered sufficient protection against diffuse reflections of the laser light, but extreme care had to be taken not to directly view the laser beam.

A Class IV laser warning sign and a rotating amber warning light identified the room as a Class IV laser hazard. The warning light was turned on whenever the laser was powered up. A fire extinguisher was positioned in the experimental area in case of fire. Finally, a safety standard operating procedure was written and submitted for approval to the Naval Postgraduate Radiation Safety Officer.

B. LASER SELECTION AND SETUP

1. Synrad Laser

The laser we selected for the laser radar configuration was the Synrad Model G48-1-28(W) 10.6 μ m CO₂ laser. Synrad rated the laser at 10 Watts. The laser required a 28 Volt DC power supply to power the laser. We choose the 28 VDC powered laser to facilitate possible field use of the laser. Table 3-2 shows the operational settings for the

	Voltage (Volts DC)	Current (Amps)	Notes
Pre-operation	28.0	0.04	<ul style="list-style-type: none"> • Key switch turned off. • Power Led is off. • Control TTL voltage is off.
Stand By	28.0	0.37	<ul style="list-style-type: none"> • Key switch turned on. • Power Led is on. • Control TTL voltage is off.
Operational	28.0	up to 9.85 observed	<ul style="list-style-type: none"> • Key switch turned on. • Power Led is on. • Control TTL voltage is on. • Five second delay circuit active. • Red Lase LED is on. • No lasing occurs.
Steady State Operational	16.0-28.0	5.05 to 5.36 observed	<ul style="list-style-type: none"> • Key switch turned on. • Power Led is on. • Control TTL voltage is on. • Lasing occurs. • Red Lase LED is on. • Laser power controlled by DC Voltage applied.

Table 3-2 Laser Operational Settings

laser. A 5 Volt TTL voltage source provided by an HP-6216A power supply controlled the lasing action. A pulsed TTL control voltage would pulse the laser while a continuous TTL signal would provide a continuous wave laser beam. When operating as a continuous wave laser, the laser power output could be controlled by varying the amount of DC voltage the laser received. We used an HP-6038A power supply to provide the DC voltage to the laser. This power supply continuously displayed the voltage and current the laser was drawing. It also allowed the operator to set the maximum voltage and current the laser could receive. The laser has several different voltage and amperage settings based on its operational status. The TTL signal applied to the laser in the stand-by mode would activate a safety circuit that allowed five seconds before the laser would begin to lase. Once the laser counted off five seconds the laser would begin drawing an increased current. The observed current levels reached over nine and a half amps before the laser would reach threshold and begin to lase. The laser drew over five amps when it reached its steady state operating conditions. The DC voltage controlled the lasing power when it was in steady state. Figure 3-2 shows the front, rear and side views of the laser. The DC

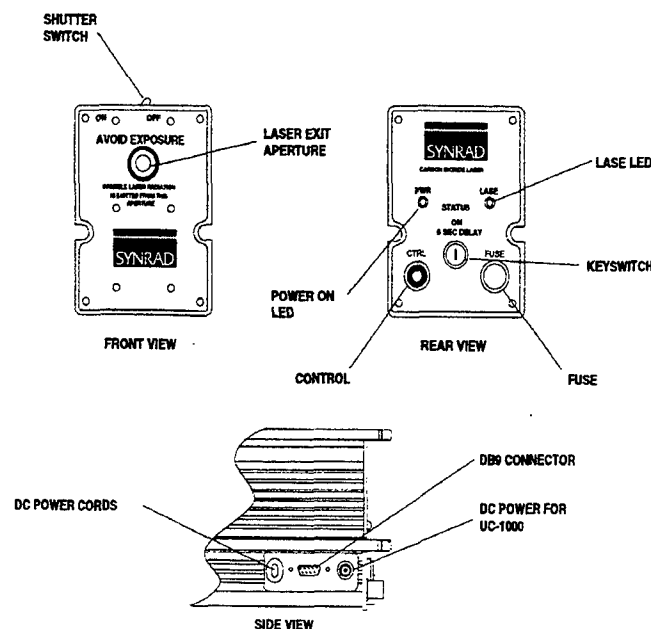


**Figure 3-2 Synrad Laser Physical Features
Diagram (Synrad, 1996)**

power supply was hooked up to the side DC power cords. The TTL power supply was connected to the control port on the rear panel of the laser.

2. Laser Cooling

The Synrad laser used in this experiment required air cooling. Water cooled versions were available. However, we choose the air cooled laser configuration to facilitate possible field use of the laser in the future. In retrospect, the water cooled version may have been the better choice since the acousto-optic modulator also required water cooling. Placing the acousto-optic modulator and laser on the same water cooling system would have simplified the laser radar design and eliminated any possible vibration transmission from the cooling fans. The laser can still be modified to a water cooled configuration with an add on water cooling kit from Synrad.

Using the air cooled configuration requires a total air flow of 500 cubic feet per minute. We used four 4.5 inch fans that ran off of 110 VAC. These fans were cheap and readily available. They were placed on a frame and suspended above the laser by a suspension system that was mounted to the wall. Figure 3-3b shows the laser placed on a

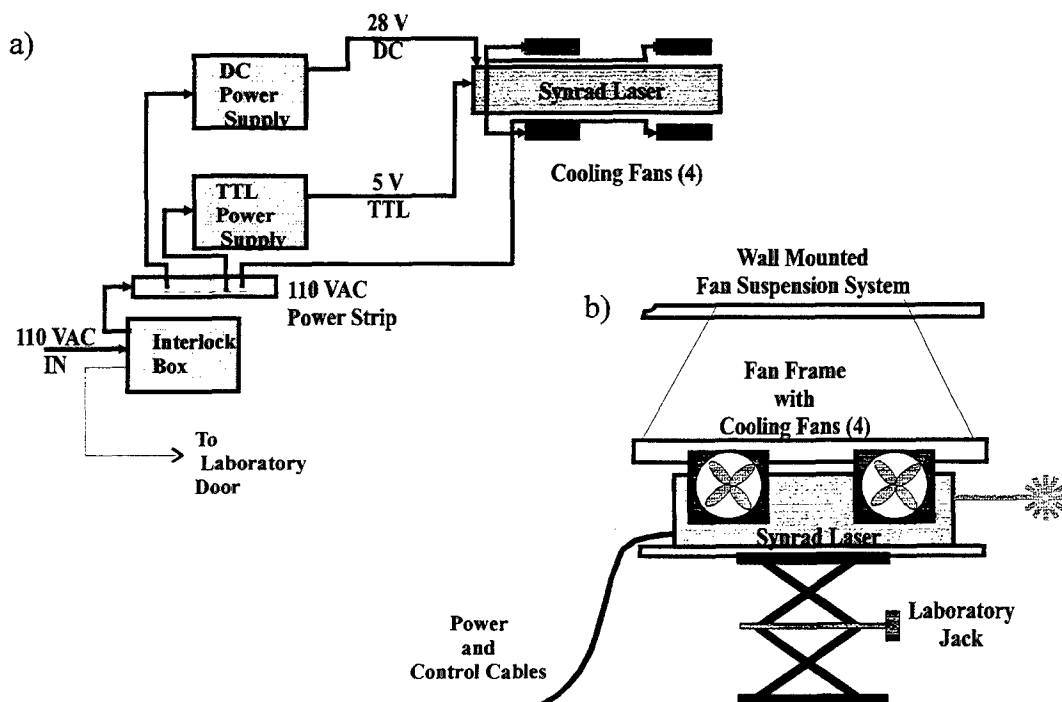


Figure 3-3 Laser Power Cooling Configuration

laboratory jack that allowed vertical positioning within the laser radar system. The cooling fans were suspended so that they did not touch the laser. This isolated their vibrations from the rest of the laser radar system.

The power distribution is shown in Figure 3-3a. The interlock box controls the laser power supply, control voltage and cooling fans. If the laboratory door was opened inadvertently, the interlock box would shut down the laser system automatically.

C. OPTICAL BREADBOARD

The laser radar system needed to be isolated from normal laboratory vibrations. The optical breadboard provided a way to attenuate these vibrations, minimizing their influence on our laser radar. It also provided a means to accurately position lenses and equipment. Elaborate systems exist from a number of manufacturers. The more elaborate optical breadboards were more expensive. We selected a TMC four inch thick optical breadboard (Series 78) with $\frac{1}{4}$ -20 threaded holes on one inch centers. The optical breadboard was matched to the available laboratory table size. This gave us a working space of approximately 2' x 5'. A second smaller optical breadboard was also purchased. This breadboard was the two inch optical breadboard (Series 78) table with $\frac{1}{4}$ -20 threaded holes on one inch centers. The size of this bread board was 1'x 2'. We used this breadboard to isolate the target from the rest on the laser radar system.

The performance of these optical breadboards is measured by their compliance factor. Compliance is the reciprocal of the dynamic stiffness of the bread board. It is the ratio of displacement to force as a function of the force's frequency. The manufacturer lists a compliance range of 10^{-5} in./lb. force to 10^{-7} in./lb. force for our breadboards (TMC, 1996).

D. ACOUSTO-OPTIC MODULATOR CONFIGURATION

The acousto-optic modular (AOM) was configured to provide a frequency shift to the laser beam. We used an Interaction Corp. AOM (Model AGM-406B1) combined with a 30 Watt 30 MHz RF power supply (Model GE 3030). Figure 3-4 shows the basic

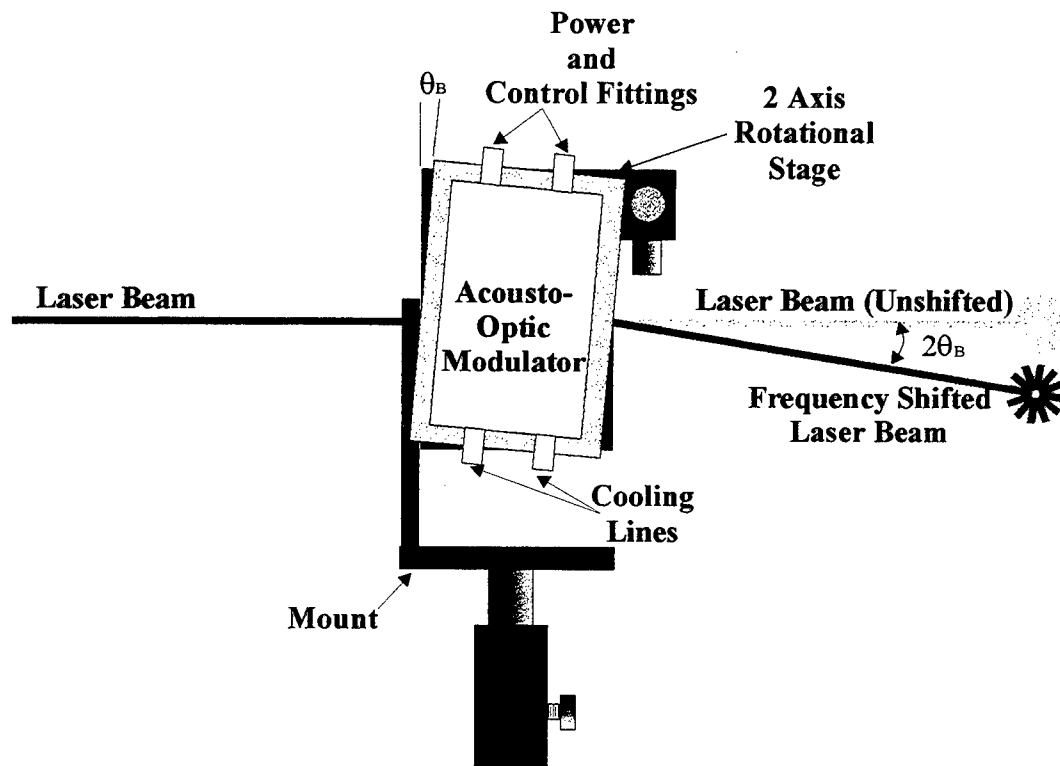


Figure 3-4 Acousto-Optic Modulator Configuration

configuration. The AOM was mounted to a Newport two axis rotational stage allowing us to control the orientation of the AOM with respect to the inbound laser beam. The AOM was water cooled requiring a supply of water of about four gallons per hour (Interaction Corp. 1996). This was provided by a small pump and water supply system. The RF power driver was connected to the top of the modulator along with a control line that provided emergency shut off of the AOM if the AOM crystal overheated. The orientation angle of the AOM was adjusted to match the Bragg angle θ_B . The Bragg angle of 28.91 mrad is required to achieve the maximum efficiency in frequency shifting the laser beam. The easiest way to achieve this angle was to set the RF driver to maximum

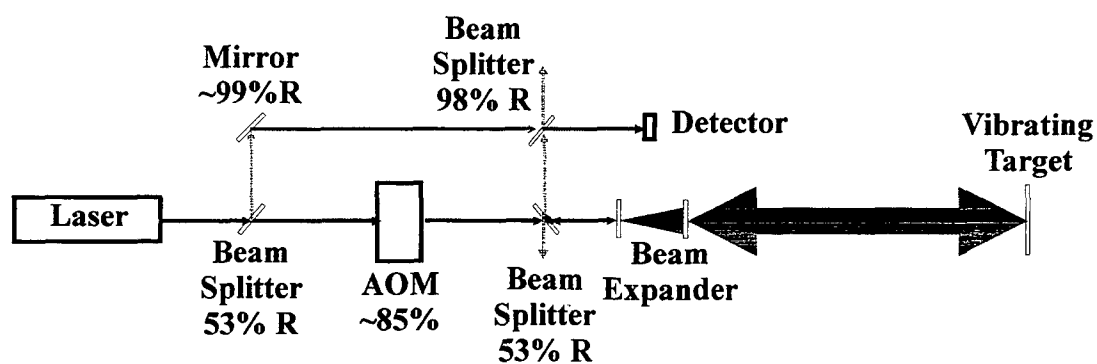
power, 30 Watts, and adjust the angle of the AOM while observing the two output beams. The output beams can be observed using special IR beam probes. Adjusting the angle of the AOM changes the output of the two beams. As the AOM nears the Bragg angle, the frequency shifted beam will grow in intensity while the unshifted beam decreases. Maximizing the output of the frequency shifted beam is desired.

The polarization of the laser beam is also important to know. The most efficient operation of the AOM occurs when the polarization of the beam is parallel with the base of the AOM. Our laser produced an S-polarized beam requiring the AOM to be oriented vertical as shown in Figure 3-4. In this configuration, efficiencies of above 80% were observed. The unshifted beam was then blocked by a spatial filter.

E. LENS SETUP

1. Design Considerations

The lenses and windows used in our laser radar configuration were made of Zinc Selenide. Figure 3-5 shows the configuration used in our experiment. This material is transparent at $10.6\mu\text{m}$. Normal glass cannot be used as a lens since it is not transparent at this wavelength. Zinc Selenide lenses average about 300 dollars each. Beam Splitters,



$$\text{Optical Transmitting Efficiency} = (0.53)(0.85)(1 - 0.53) = .21 \text{ or } 21\%$$

$$\text{Optical Receiving Efficiency} = (0.53)(0.98) = .52 \text{ or } 52\%$$

Figure 3-5 Optical Configuration

with their precise reflectance controlled by special coatings, can run as high as 1800 dollars each. Design of the laser radar optics system must consider these costs. The ideal optical configuration transmits as much laser light towards the target as possible while attenuating the returning signal as little as possible. In our configuration, the laser radar transmits 21 percent of the laser power towards the target. The system is able to apply 52 percent of the laser power received by the collecting lens assembly to the detector. This laboratory configuration could be modified to make the optical efficiencies higher. The beam splitters we purchased from II-VI Corporation were partial reflectors with a sight six to ten arc minute wedge between the two surfaces. One surface was coated with an antireflective coating while the other surface was coated with a reflective coating designed to reflect a standard percentage of 10.6 μm light at zero degrees incidence. II-VI was able to measure the S and P polarized reflectances at 45 degrees. This gave us ball park numbers for reflectance when we used these partial reflectors as beam splitters. This is why the reflectance values are not standard values of 20, 30, 40, etc. percent. To achieve those exact values requires special coating runs and drives the price of the beam splitter up to the \$1800 range. For our purposes, the partial reflectors used as beam splitters achieved our purpose at a fraction of the cost.

2. Lens Mounts

The lenses and beam splitters were all a standard 25 mm diameter. They were mounted in Melles Griot gimbal mirror and beam splitter mounts. The gimbal mounts allowed ± 7 degrees of tilt about two orthogonal axes with an angular resolution 10 arc seconds. These gimbal mounts were mounted to posts designed to fit into an Edmund Scientific post and rail system. Two rails were used. The first rail contained the first beam splitter that split the local oscillator off from the main beam, as well as the AOM and beam expander lenses. The detector, local oscillator turning mirror and recombination beam splitter were mounted on the second rail.

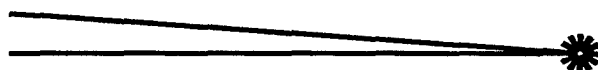
3. Coincidence and Parallelism of the Beams

The optical alignment is critical to the operation of the laser radar. The goal in aligning the reference or local oscillator beam and the target beam is to make them as parallel as possible and coincident. Figure 3-6 illustrates these concepts. In Figure 3-6a

a.) Non-Parallel, Non-Coincident Beams



b.) Non-Parallel, Coincident Beams



c.) Nearly Parallel, Coincident Beams



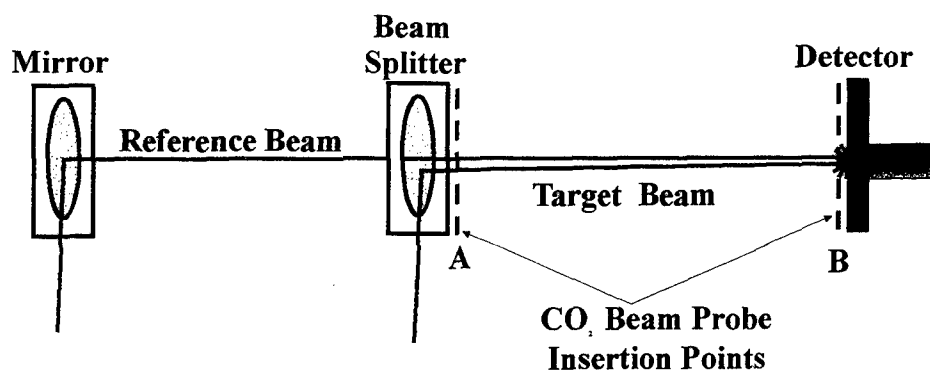
Figure 3-6 Optical Alignment

the two beams are neither parallel nor coincident. Interference can not occur at the detector. Figure 3-6b show coincident beams but with low heterodyne efficiency. The more parallel the coincident beam are, the higher the heterodyne efficiency. Figure 3-6c shows the beams approaching the desired configuration. The maximum desired angle between the two 1mm diameter beams was calculated in chapter two. The beam

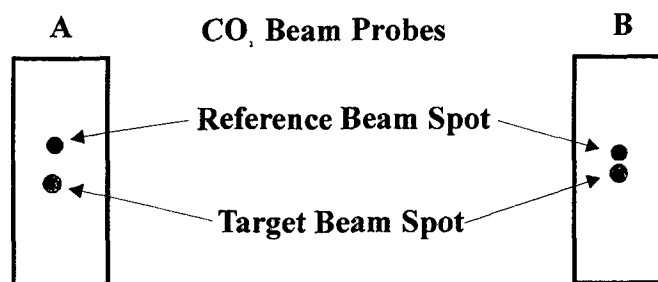
diameters involved in our system were about 5mm which made the desired maximum angle between the two beam about 1 milliradian.

The simplest way to achieve this small angle is shown in Figure 3-7. The beam

a.) Detector Rail Lens Alignment



b.) CO₂ Beam Probe View Before Alignment



c.) CO₂ Beam Probe View After Alignment

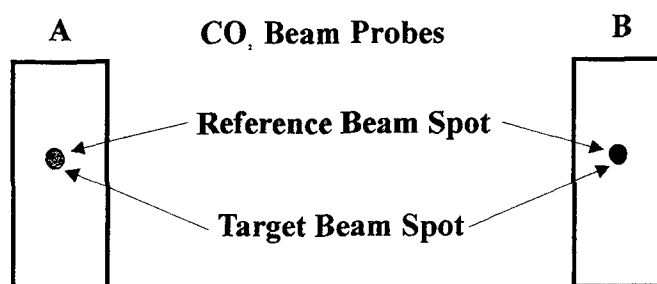


Figure 3-7 Beam Alignment

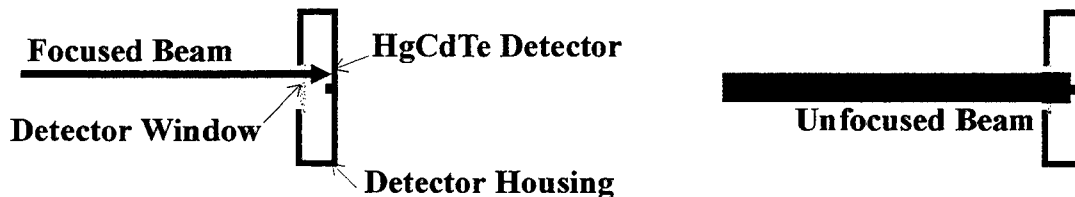
locations were measured at two locations using Macken Inc. CO₂ laser beam probes (Model 23S) as shown in Figure 3-7a. These beam probes allow us to view the infrared beams. They require an ultraviolet light source to illuminate the surface of the beam

probes. The 10.6 μm light hitting the beam probe showed up as a dark spot on the beam probes. This allowed us to observe the beams at two points, A and B. Ideally these points should be as distant as possible. Basic geometry dictates that the greater the distance between the detector and beam splitter the more accurate adjustments we can make. The gimbal mounts were then adjusted so that the reference beam and target beam coincided at both points A and B Figure 3-7b and Figure 3-7c.

Aligning the beam onto the detector presents another problem. The detector is only 1mm by 1mm square. It sits behind a window in the detector housing. It was therefore hard to know precisely where the detector element was without time consuming trial and error adjustments or disassembling the detector and risk damaging the element in the process. The easiest method of aligning the coincident spot on the detector was to leave it unfocused. This allowed the coincident beam spot size to be approximately 10 mm in diameter. The beam was then centered on the detector window, guaranteeing the detector would receive at least some of the combined beam's illumination. Figure 3-8a shows the problem with a narrow or focused beam. The beam can actually miss the detector. Wide beams will hit the detector but have less power per area. For laboratory set up, the wide beam allows quick setup. For field operations the focused beam allows the detector to receive as much of the available beam as possible. This is critical when the target is at long ranges and the returning signal is weak. This will require proper time consuming alignment. The other option is to use a more sensitive detector with the wider beam. The system's maximum potential is reached when the most sensitive detector is used with the focused beam.

The last consideration in the beam alignment is to beware of the unshifted beam coming out of the acousto-optic modulator. This beam travels along the same line as the original beam. Spatial filtering prevents the unshifted beam from propagating out of the system. Figure 3-8b shows a simple way of stopping this beam. The beam is effectively stopped by adjusting the beam splitter and lens mounts so the unshifted beam hits the mount instead of passing through the lens.

a.) Beam Alignment on the Detector



b.) Simple Spatial Filtering of the Unshifted Beam

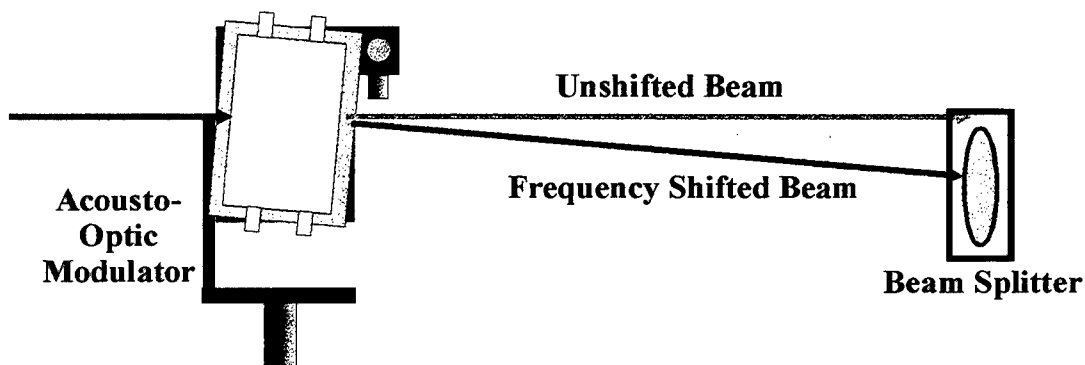


Figure 3-8 Beam Alignment on the Detector

F. TARGET CONFIGURATION

In order to evaluate the laser radar's performance in the laboratory, a special target was needed. It was desirable to control and know the target's vibrational frequency and amplitude. Piezoelectrical systems allowed us to construct an inexpensive (less than \$1000) controllable vibrating target.

1. Piezoelectronics

Materials used in piezoelectronics have an asymmetric charge distribution within their molecular structure. When a voltage difference is applied to the material the result is an expansion of the material. The amount of voltage difference applied to the material controls the amount of expansion that occurs in the cell. Piezoelectric material

manufacturers combine this type of material into piezoelectric stacks of many different configurations. The total displacement is thus a function of the voltage difference and the number of stacks. The material will return to its original size when the voltage difference is dropped to zero. Figure 3-9 shows the relationship between voltage applied to the piezo stack used in our target and the amount of displacement achieved in the material.

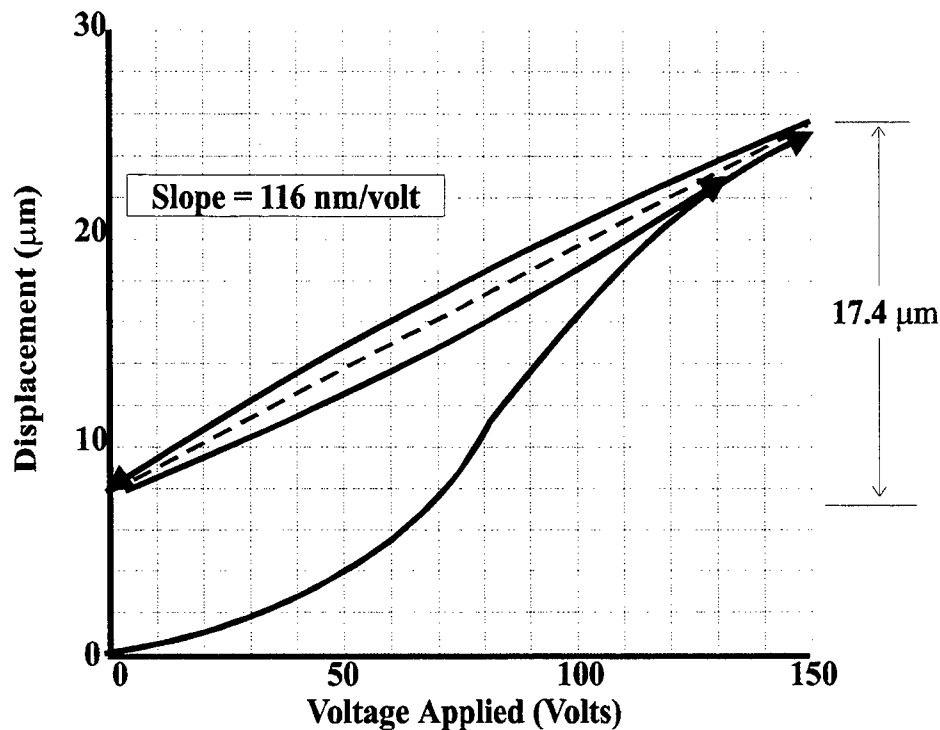


Figure 3-9 Piezoelectric Displacement vs. Voltage (Thor Labs, 1996)

The piezoelectric actuator used in our target was the Thor Labs Model PE4. This actuator was enclosed in a stainless steel case that allowed 17.4 μm of displacement when driven by a sinusoidal voltage. The actuator does not relax completely when the applied voltage is reduced to zero. The displacement is thus the difference between the high and low voltage states. The PE4 is capable of 17.4 μm of displacement when a 0-150 V difference is applied. The displacement can be expressed as a function of this applied voltage when driven by a sinusoidal voltage. The slope of the displacement curve gives us a reasonably accurate measurement of displacement of the tip of the piezoelectric stack.

The slope of 116 nm/volt was derived from the Thor Labs specification sheet from the PE4 (Thor Labs, 1996). There is hysteresis involved during the displacement. This hysteresis contributes to the inaccuracy in the position of the actuator tip. Under normal conditions this error is about 15%.

2. Piezoelectric Response Times.

The response time frequency limit of the piezoelectric stack is determined by the resonant frequency of the piezoelectric "target configuration." In our case, this is the resultant resonant frequency of the combined piezoelectric stack and retro-reflector. The resonant frequency of the piezoelectric stack alone is 68,000 Hz (Thor Labs, 1996). To estimate the change in the resonant frequency due to adding the mass of the retro-reflector we used the following effective mass equation (Physik Instrumente, 1996)

$$f_r = f_r \sqrt{\frac{m_p}{m_p + 2M_r}}, \quad (3-1)$$

where f_r equals the new system resonant frequency, f_r equals the resonant frequency of the piezoelectric stack alone, m_p equals the mass of the piezoelectric stack and M_r equals the mass of the retro-reflector.

The retro-reflector was obtained from Edmund Scientific part number C43,652. It has a mass of 32 grams. The mass of the piezoelectric stack was 4.8 grams. This resulted in an estimated target configuration resonant frequency of approximately 18,000 Hz. Thor Labs states that the fastest response time the cell could handle is

$$T_{\text{response}} = \frac{1}{3f_r}. \quad (3-2)$$

Thus the system had a response time of 18.5 μ m seconds. The corresponding highest frequency the piezoelectric stack could faithfully match is approximately 54,000 Hz.

3. Piezoelectric Stack Strength Limitations

The physical strength of the piezoelectric also needed to be considered. The PE4 had a limiting strength of 850N (Thor Labs, 1996). We used a sinusoidal driving function. The maximum associated frequency that could be achieved without tearing the piezoelectric stack apart is expressed by

$$f_s = \frac{1}{2\pi} \sqrt{\frac{S_l}{A}}, \quad (3-3)$$

where S_l equals the limiting strength of the piezoelectric stack and A equals the amplitude of vibration in the target.

For the maximum amplitude of vibration of 17.4 μm , the maximum frequency the piezoelectric stack can physically handle would be approximately 1,110 Hz. For a 1 μm amplitude displacement the piezoelectric stack could handle approximately 4,600 Hz.

4. Piezoelectric Current Requirements

The piezoelectric stack also has a capacitance associated with it. This capacitance can also act as a limitation on the maximum frequency the target can achieve. For a given current, the maximum frequency is

$$f_i = \frac{I}{2CV_D}, \quad (3-4)$$

where I equals the current applied to the piezoelectric stack C equals the capacitance of the piezoelectric stack and V_D equals the voltage applied to the piezoelectric stack.

The capacitance of the piezoelectric stack was given by Thor Labs as 1.40 μF . A signal generator used to create the sinusoidal displacement did not have the current capabilities to drive the piezoelectric stack. Its signal was input into a Thor Labs amplifier Model MDT 691. This amplifier was capable of 60mA. This amplifier would allow the target receiving a voltage of 150 volts used to achieve 17.4 μm maximum displacement to vibrate at 143 Hz. For a smaller amplitude vibration of 1 μm the achieved target vibrational frequency that could be achieved would be 2485 Hz.

The limiting factor in the capability of the target to achieve high frequency large amplitude vibrations is the amplifier. Higher power amplifiers could be used to provide higher frequencies, up to the maximum physical strength of the piezoelectric stack. Our experiment involved low frequency vibrations under 1,000 Hz with vibrational amplitude in the tens of nanometers. Therefore the target was capable of meeting our needs. The target's design is shown in Figure 3-10. The MDT-691 piezoelectric controller provided

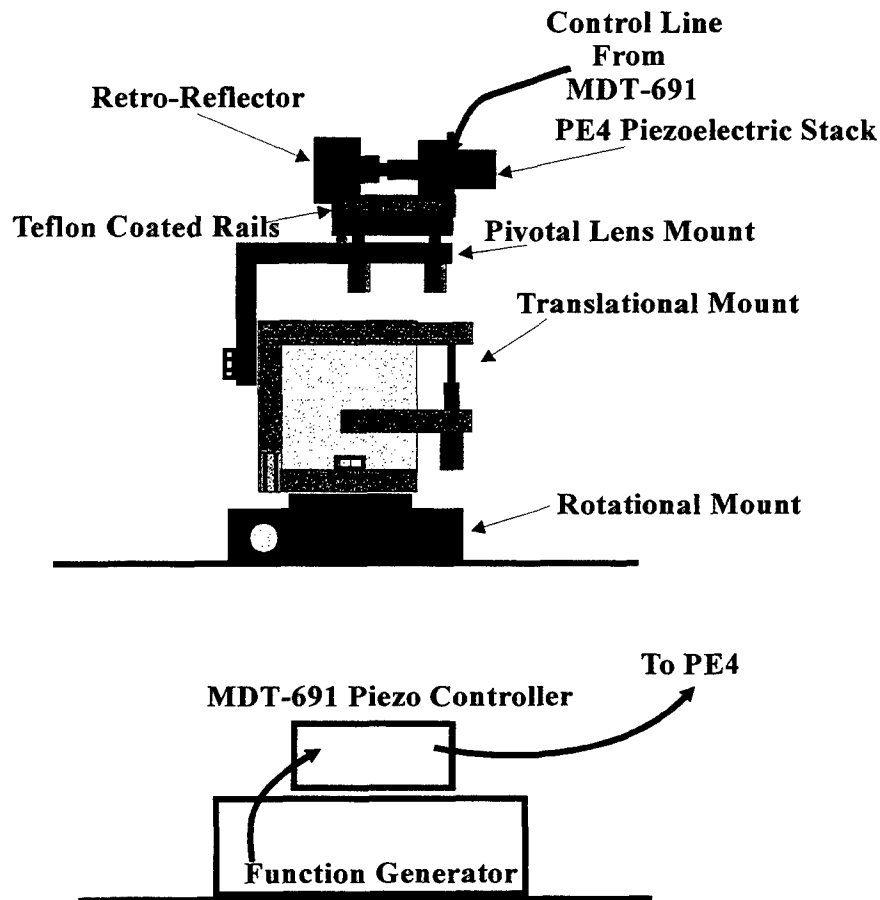


Figure 3-10 Target Design

up to 60 mA of current while multiplying the voltage received from a sine wave generating function generator. The voltage from the function generator was amplified by 15V/V to obtain the voltage supplied to the PE4 piezoelectric stack (Thor Labs, 1996). The

function generator was set up to provide a positive voltage by adjusting the offset voltage. Thus a function generator sinusoidal voltage of 0-1 volt would mean a vibrational amplitude in the target of $1.74 \mu\text{m}$.

G. ELECTRONICS

Figure 3-11 shows our electronics configuration. The electronics within the laser radar converted the frequency modulated light into an amplitude modulated voltage that could be processed by a signal analyzer to display the signal in the frequency domain.

The coincident beam hitting the detector is converted into a current signal by a Belov Technology HgCdTe detector (Model B10R-40). This was a room temperature

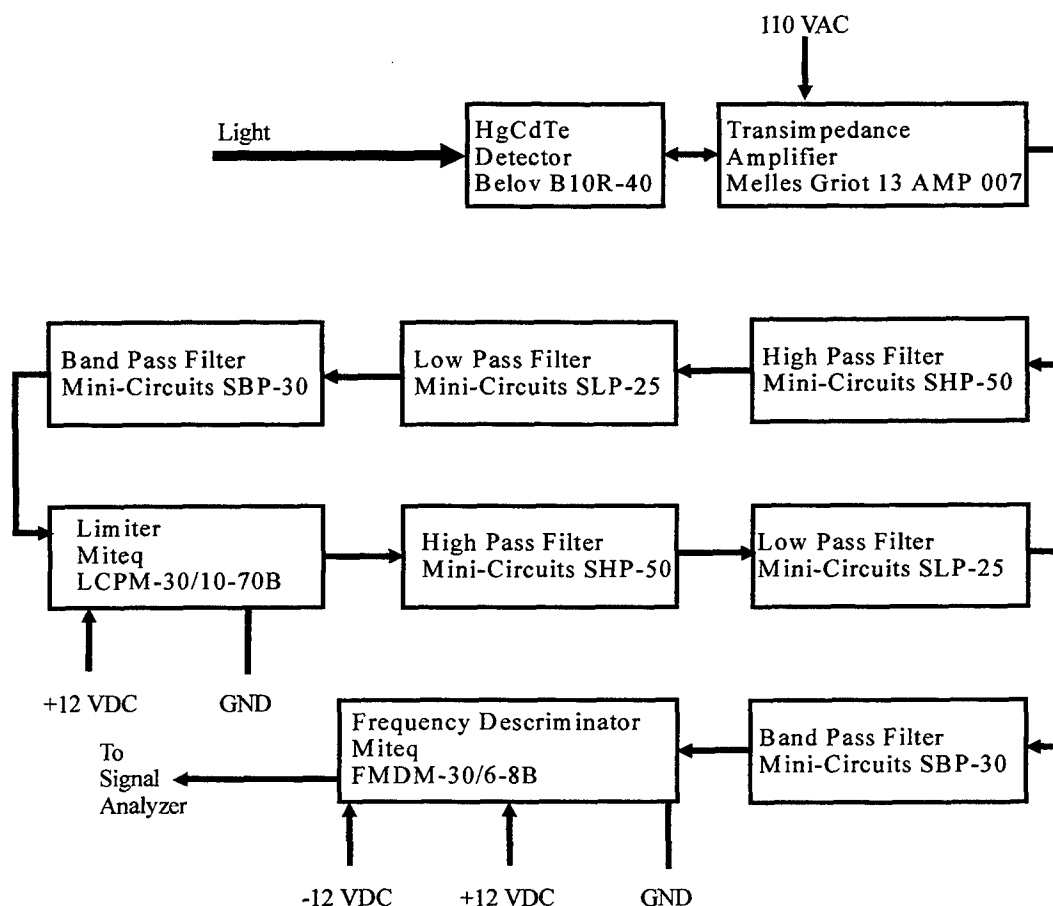


Figure 3-11 Electronic Configuration

detector that needed no special cooling. This was ideal for laboratory work where the signal returns were high. For field work a liquid nitrogen cooled HgCdTe detector with its higher sensitivity would be the ideal detector. The signal hitting the detector is a frequency modulated signal that must be amplified by a transimpedance amplifier that converts the current signal into a voltage signal. We used a Melles Griot high frequency amplifier (part number 13AMP007) to provide a transimpedance gain of 6,250 V/A over a frequency range of 4 kHz to 400 MHz (Melles Griot, 1995/1996). This amplifier also provided the biasing needed to make the detector work.

Filters were added to restrict the frequency range and improve the performance of the system. We used Mini-circuits high pass, low pass and band pass filters (part numbers SHP-25, SLP-50 and SBP-30 respectively) both before and after the Miteq limiter. The low pass filters had a -3dB passband of 0 to 55 MHz (Mini-circuits, 1996). The high pass filters had a -3dB attenuation point of 25 MHz. The band pass filter was centered at 30 MHz with an elliptical response 3dB bandwidth of 10 MHz (Mini-Circuits, 1996). These were placed after the transimpedance amplifier. While a tighter bandwidth around 30 MHz is more desirable, these filters were inexpensive and readily available. SAW filter technology could provide a tighter bandwidth and therefore better system performance but they were not readily available with a center frequency of 30 MHz. The cost and time associated with designing and making these SAW filters was prohibitive for our experiment.

A Miteq limiter (Model LCPM-30/10-70B) was used to help stabilize fluctuations in signal amplitude. These fluctuations can cause variations that the frequency discriminator will translate into amplitude variations distorting our frequency readings. These amplitude variations can come from the inside the laser radar (power fluctuations, thermal heating etc.) or outside the laser radar (atmospheric turbulence, change of target reflectivity, etc.) It is important to limit these fluctuations in signal amplitude. The limiter provides us with the ability to limit and stabilize these fluctuations. It also acts as an amplifier. Signal inputs ranging from -65 to 5 dBm are amplified by the limiter to a constant 10.74 dBm (Miteq, 1996). The frequency range is centered on 30 MHz with a bandwidth of 20.9 MHz. Since the signal was amplified by the limiter, we placed another

series of filters to reduce any signals that may have been amplified by the limiter and were outside of our desired bandwidth.

The signal is fed into the Miteq frequency discriminator (Model FMDM-30/6-8B) where the discriminator converts frequency modulation in the signal into amplitude modulation. Figure 3-12 shows the typical response curve for discriminator used in our experiment.

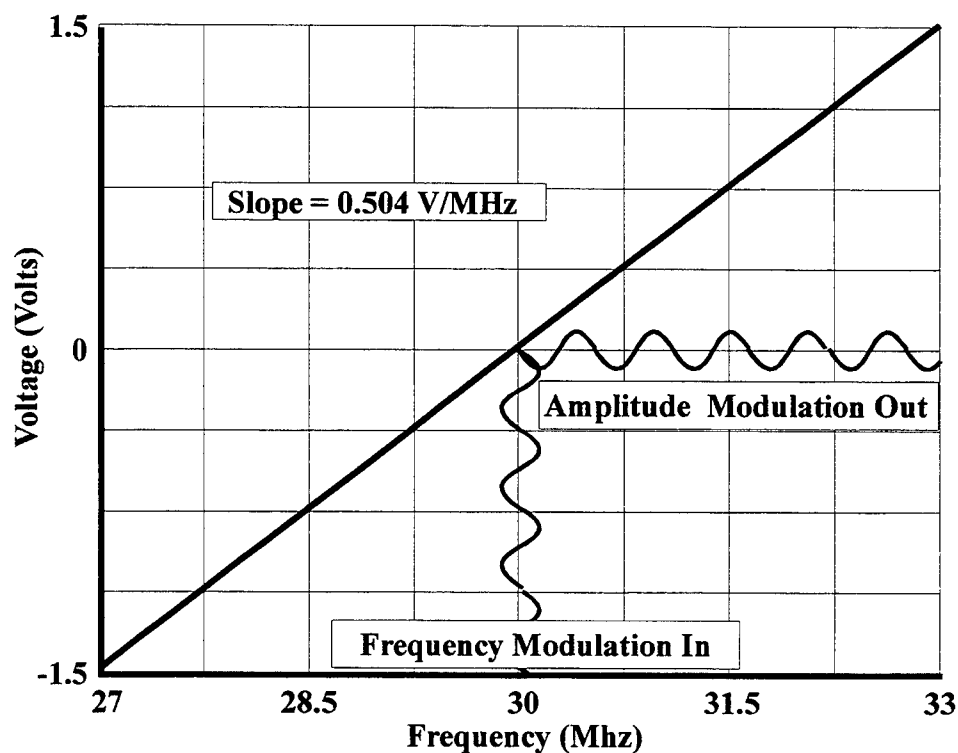


Figure 3-12 Frequency Discrimination (Miteq, 1996)

H. DATA RECORDING

We used the PM3384 Fluke digital oscilloscope to measure signal responses at various points through out our electrical circuit. The oscilloscope had the ability to perform FFTs that allowed us to view the output in the frequency spectrum. This was especially helpful during system alignment. The carrier wave at 30 MHz was easily seen by monitoring the output of the transimpedance amplifier. Once the system's lenses were adjusted, the rest of the electronics was connected. The frequency discriminator's low sensitivity of 0.504 V/MHz meant that our low frequency vibrations in the target required a much lower noise than the Fluke Oscilloscope was capable of achieving. The 400 Hz vibrations the target was producing meant that the Voltage out of the discriminator was approximately 250 μ V. The oscilloscope had to much internal noise. The target's signal was buried in the noise.

We used the Hewlett-Packard 35670A Dynamic Signal Analyzer to record the frequency spectrum data. This signal analyzer enabled us to see the vibrations caused by the target. It also allowed us to perform some basic averaging and further improve the CNR. Originally we used an HP 3585A to view the frequency spectrum. This spectrum analyzer provided excellent low noise capabilities allowing us to easily view the target's vibrational patterns. It did not have an easy means of collecting the data so we switched to the HP 35670A.

IV. OBSERVATIONS, ANALYSIS AND RECOMMENDATIONS

On 21 February 1997 we were able to detect vibrations from a target under laboratory conditions. The target's vibrational frequency and amplitude were varied and the laser radar's output was recorded. The amplitude of vibration in the target was varied from 40 nm to over 1.5 μm . The two frequencies used were 400 and 500 Hz.

A. OBSERVATIONS

The target's vibrations were easily detected by our laser radar. Figure 4-1 shows the laser radar's response for a target vibrating at 400 Hz and 1.74 μm vibrational amplitude. The signal was sampled 50 times and averaged. The averaging was not necessary for the larger amplitudes. The target's frequency was easy to detect from the noise. Averaging gave us a somewhat better picture on the smaller amplitude vibrations. The 400 Hz signal with a power spectrum measurement of -37 dBm can clearly be seen. There are other frequency responses that appear as well. The first high power frequency "spike" occurs at about 85 Hz. Frequency spikes also occur centered on the 400 Hz signal. Notice that these frequencies are 315 Hz, 379 Hz, 421 Hz and 485 Hz. These side bands appeared intermittently throughout the duration of the experiment. Side bands of 120 Hz also appeared intermittently as well. Turning the target off, stopping its vibrations, we observed the laser radar returns off of the stationary target. Figure 4-2 shows this response. Here the 85 Hz signal as well as a 21 Hz signal can be seen. Looking back at Figure 4-1 shows that these frequencies appear as fundamental frequencies (see the 85 and 21 Hz signals) and as side bands off of the 400 Hz signal (315 Hz, 379 Hz, 421 Hz and 485 Hz). The signals present are 21 Hz, 85 Hz, 400 ± 21 Hz and 400 ± 85 Hz and 400 Hz. Weaker signals of 52 Hz and 400 ± 52 Hz are also present but are less defined. To eliminate receiver noise as a possible source of these signals, we turned off the laser and monitored the systems response. Figure 4-3 shows the response with laser turned off. The detector/electronics circuit was left on. The figure clearly shows the typical 60/120/240 Hz pattern. We easily traced the cause of these signals to the 30 Watt, 30 MHz RF driver powering the AOM. By comparing Figures 4-1 through 4-3 we can conclude that the cause of the side bands must be in the laser-modulator system or be present in the ambient vibration environment of the laboratory. Equipment was not readily available to further examine either of these possibilities. Adjusting the target frequency had no effect on the side bands they showed up as 500 ± 85 Hz.

Date: 12/03/ Time: 16:25:00

A: CH1 Pwr Spec X: 485 Hz Y: -48.362 dBm

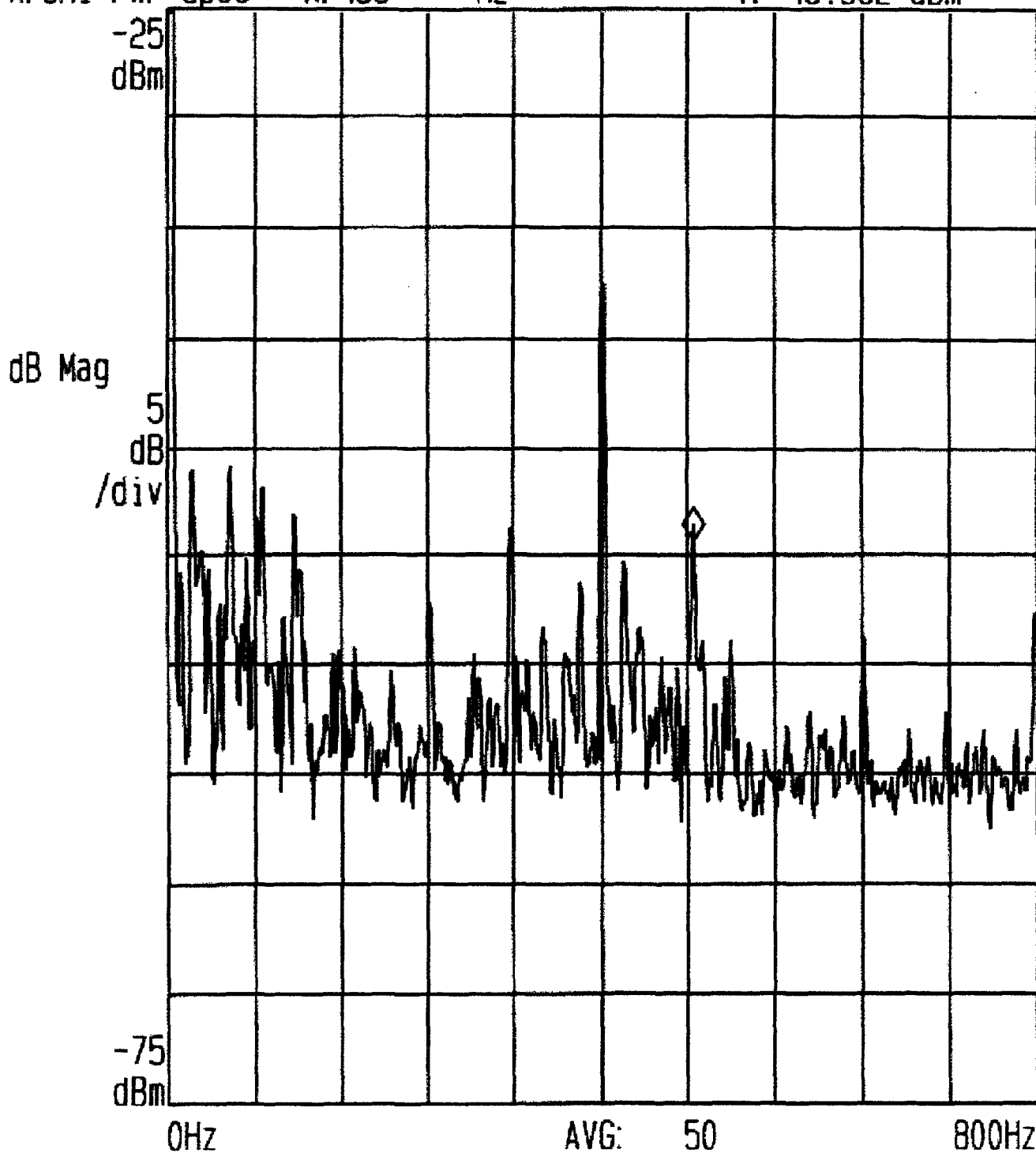


Figure 4-1 Response of the Vibrating Target

Date: 12/03/ Time: 15:52:00

A: CH1 Pwr Spec X: 86 Hz Y: -54.512 dBm

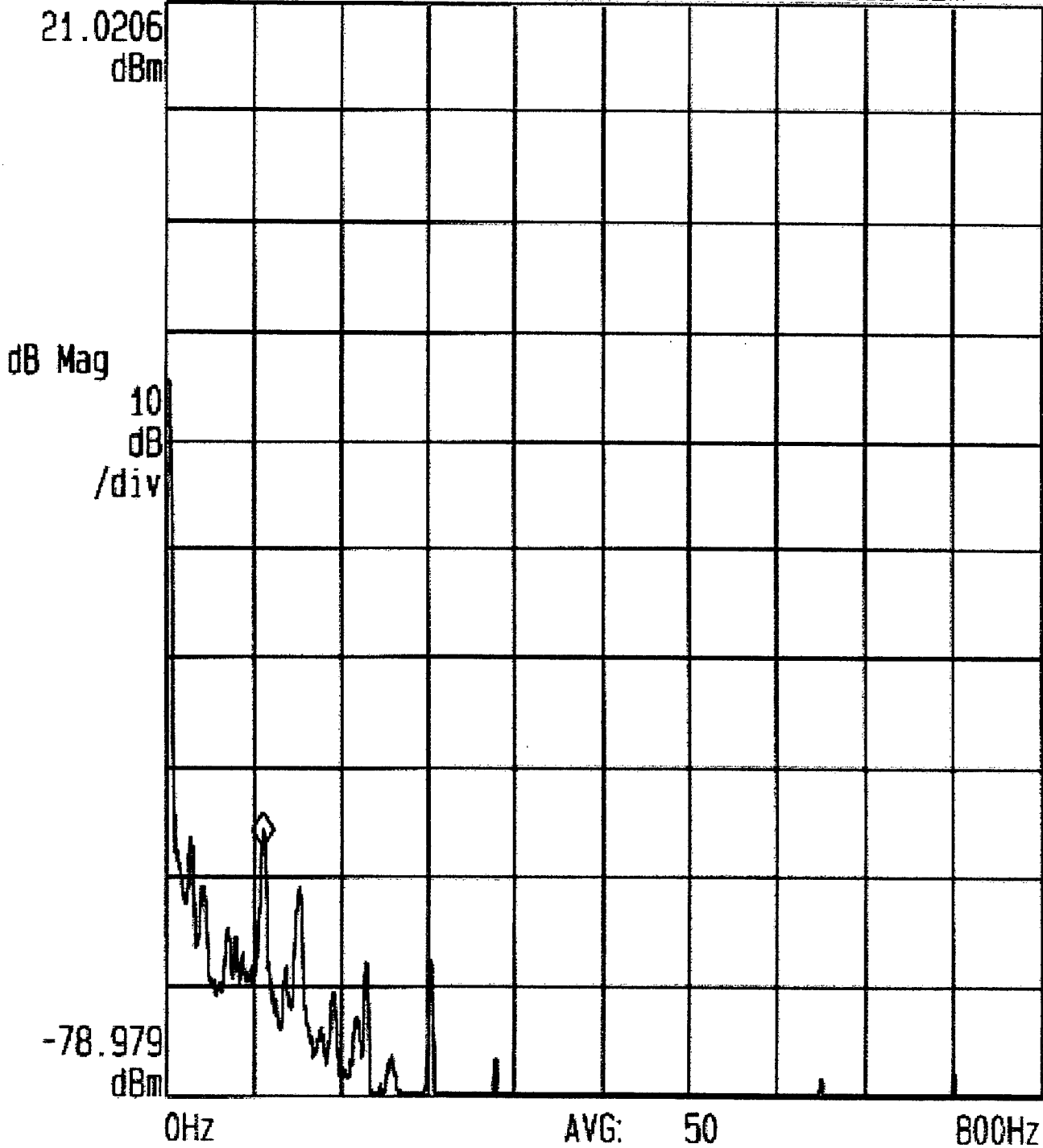


Figure 4-2 Response with Target Turned Off

Marker Fcn

Date: 21/02/ Time: 13:28:00

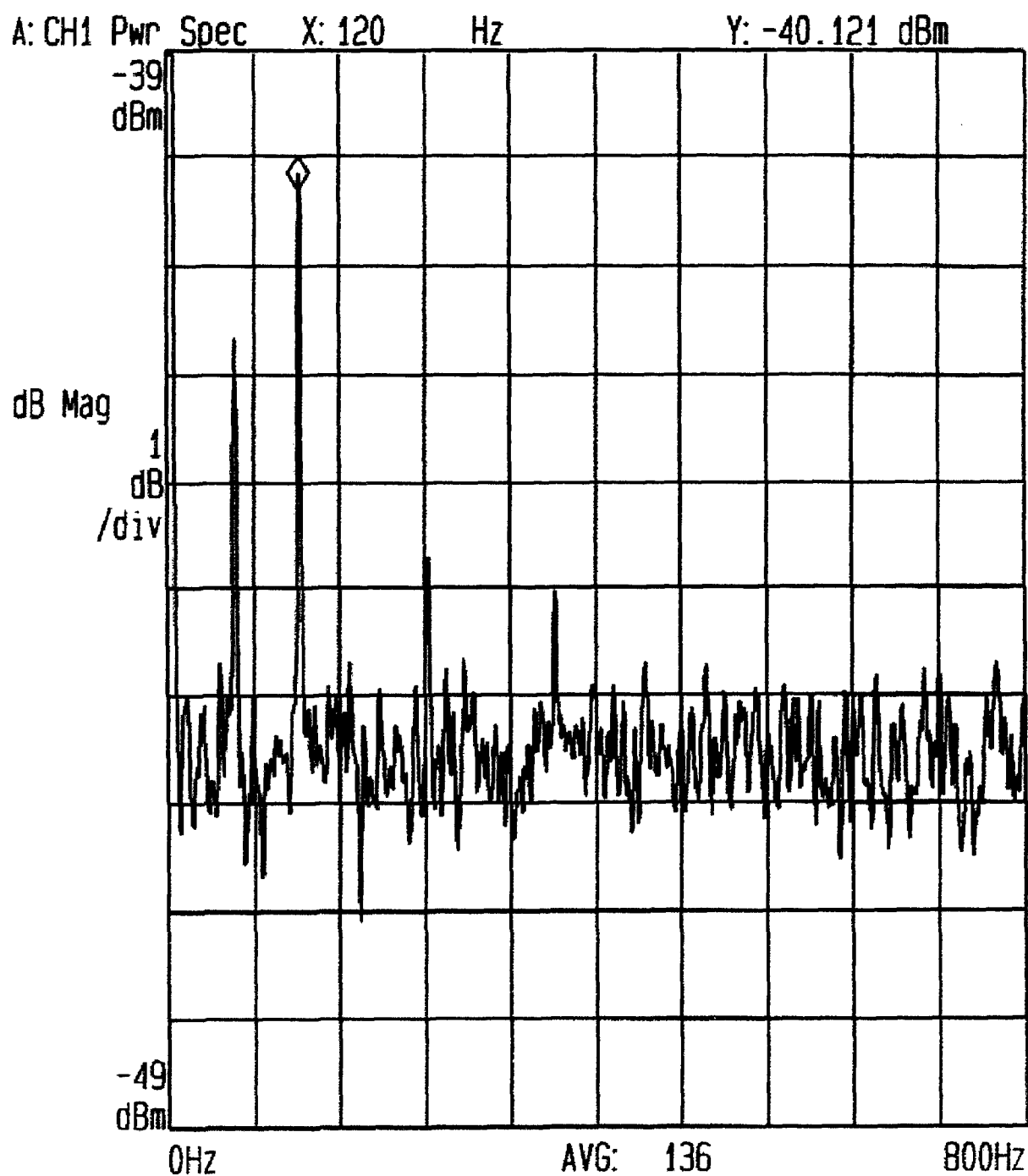


Figure 4-3 Response with Target and Laser Off

The laser radar also exhibited an intermittent jump in the power spectrum across all frequencies be observed. Figure 4-4 illustrates how this looked as we were observing the data. This power surge continued to occur despite checking the electronics and changing the signal analyzers. It persisted throughout the several days of measurements. It did not occur when the laser was turned off and we were just examining the noise in the

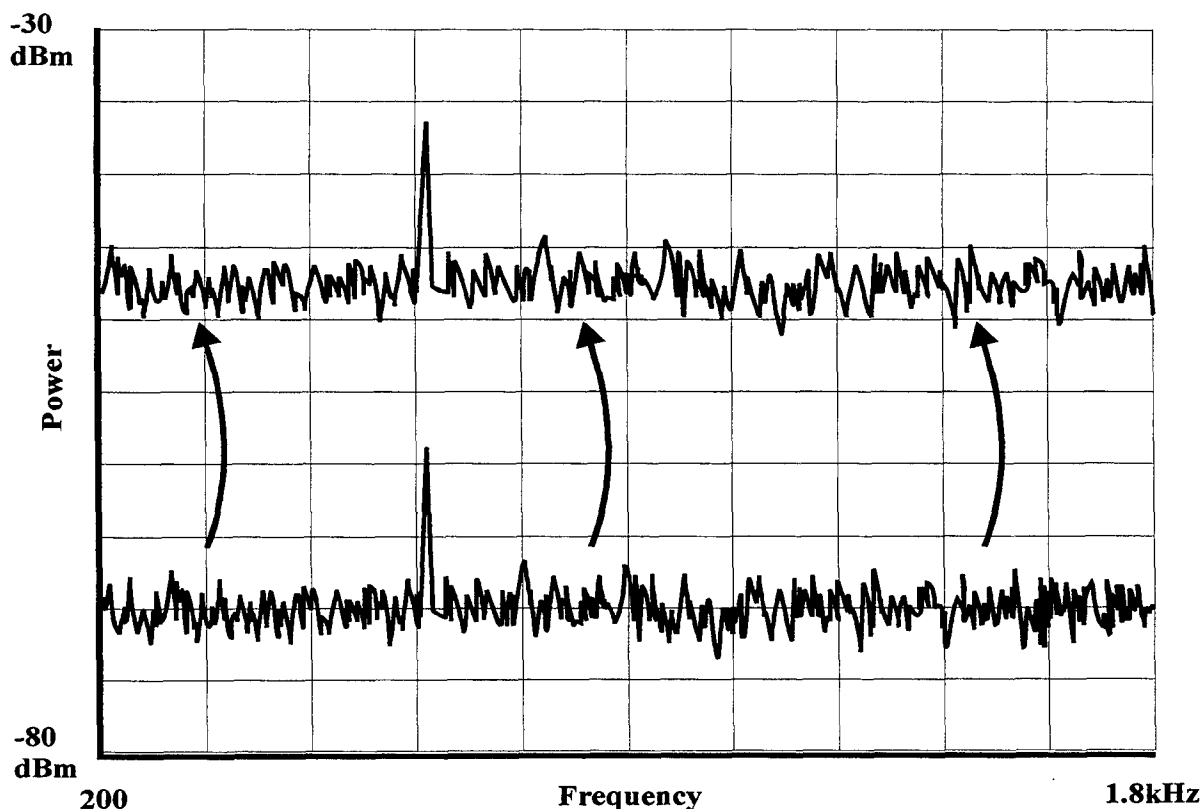


Figure 4-4 Power Surge

electronics. This would indicate that the laser or its associated electronics is a possible cause of the anomaly. One possible source is the sudden appearance of a second laser axial mode which would cause the shot noise to increase enormously without a concomitant increase in the signal. Time did not permit investigation of this possibility.

The laser radar was able to distinguish target vibrational amplitudes from about 40 nm. Figures 4-5 through 4-7 show the signal returns as the target amplitude is increased. Figure 4-5 shows the signal for a 40 nm vibrational amplitude. Figure 4-6 shows the

return for a $1\mu\text{m}$ target vibrational amplitude. Note the side bands appearing. The side bands around the 400 Hz signal are the ones already discussed. At this amplitude the 800 Hz harmonic can now be seen as the vibrational amplitude is reaching the wide band FM status. Finally, Figure 4-7 shows a target vibrating at 500 Hz and $1.74\mu\text{m}$. The 1,000 Hz harmonic can be easily seen as well as the ± 85 Hz sidebands.

Date: 21/02/ Time: 12:58:00

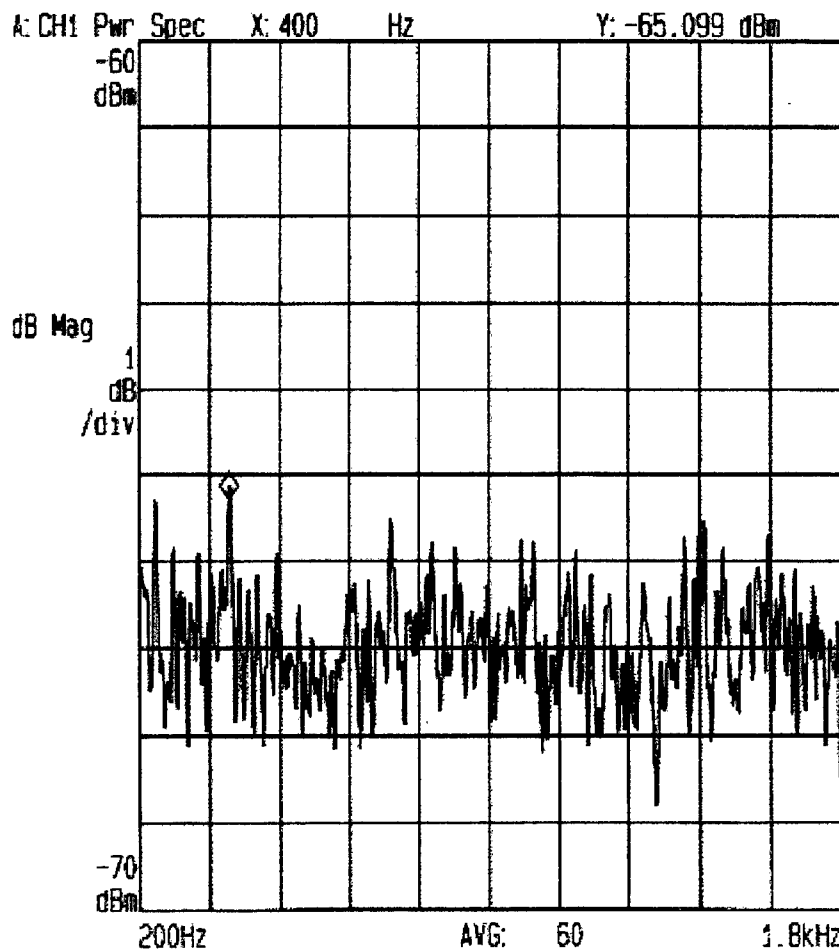


Figure 4-5 Laser Radar Return from a Target Vibrating at 400 Hz and 40 nm Amplitude

Date: 12/03/ Time: 17:28:00

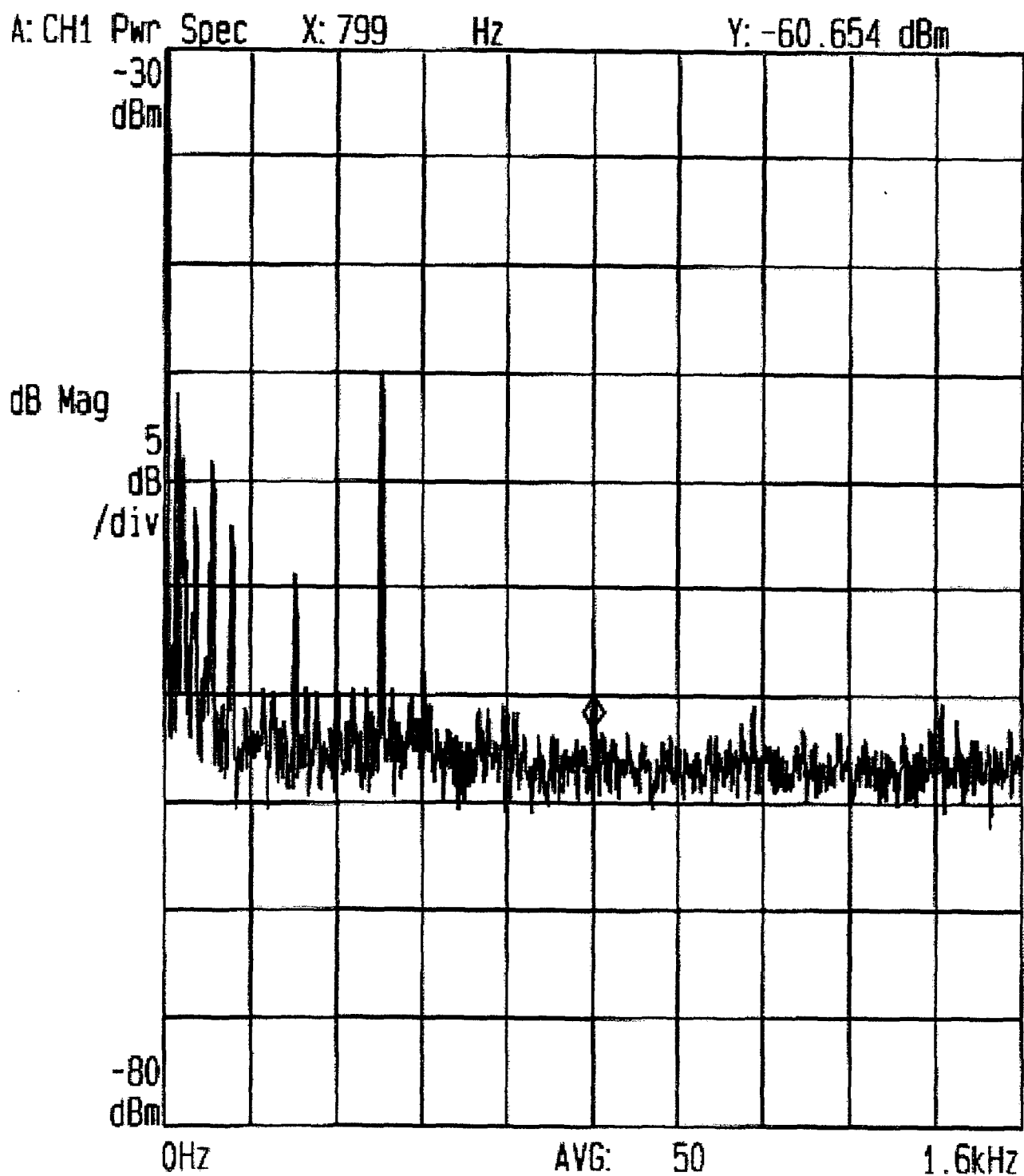


Figure 4-6 Laser Radar Return from a Target Vibrating at 400 Hz and 1 μ m Amplitude.

Date: 12/03/ Time: 17:22:00

A: CH1 Pwr Spec X: 1 kHz Y: -59.954 dBm

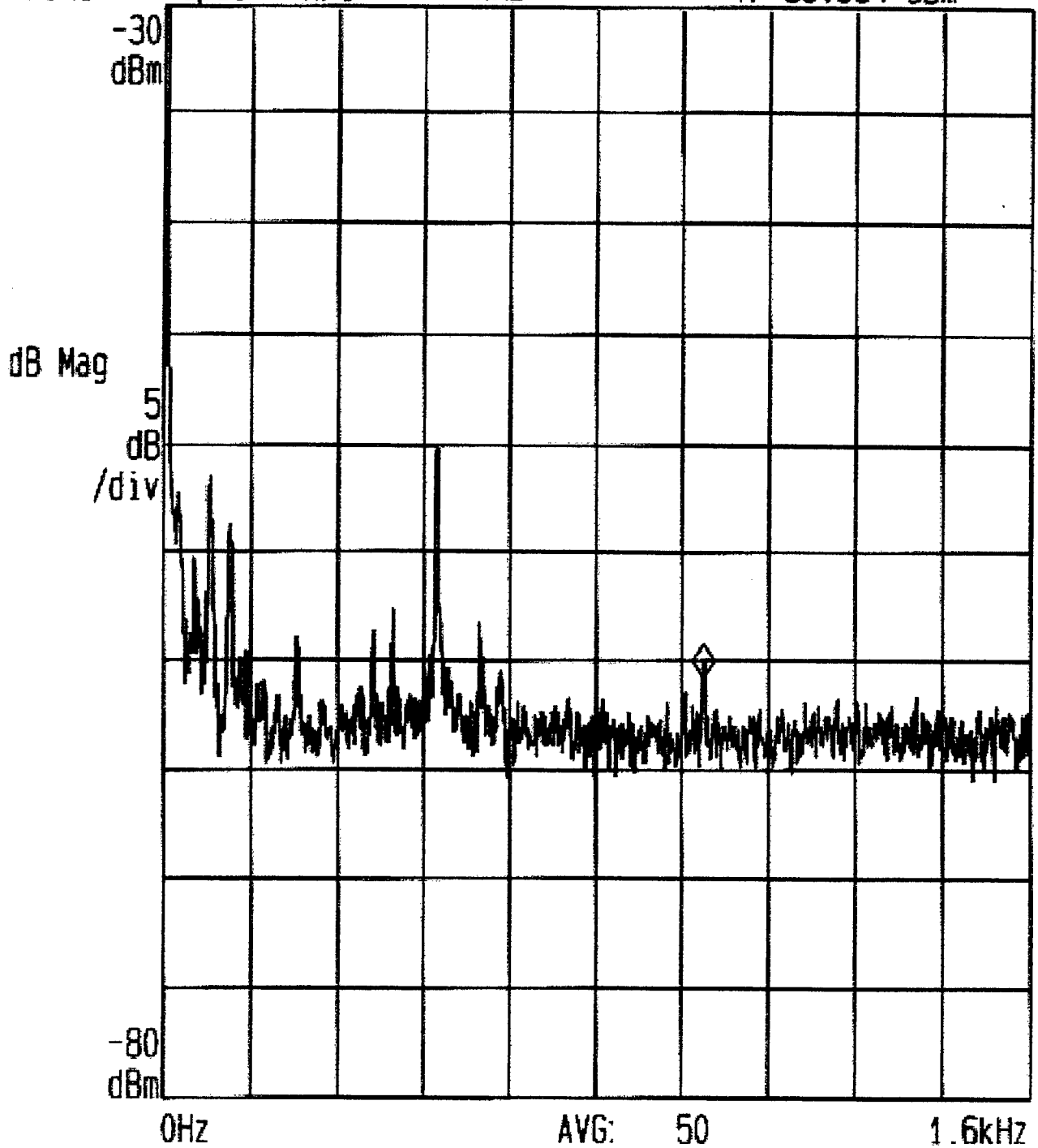


Figure 4-7 Laser Radar Return from a Target Vibrating at 500 Hz and 1.74 μm Amplitude.

B. CONCLUSIONS AND RECOMMENDATIONS

1. Measurement Capabilities

The laser radar we constructed accurately detected the vibrational frequencies in the target. It was able to detect vibrational amplitudes down to about 40 nm using simple sample averaging signal processing. We had wanted to explore the relationship between the vibrational amplitude target and the SNR observed on the signal analyzer. The relationship should be a nonlinear relationship involving the Bessel functions as a function of amplitude. If these relationships can be defined accurately it could give an additional parameter to help classify and identify targets. The power surges made it impossible to conduct this analysis.

Harmonics of the vibrating frequency appeared as the amplitude of vibration in the target was increased. The distinction between narrow band FM and wide band FM may allow for a rough approximation of the vibrational amplitude. As the amplitude of vibration increases, the signal return goes from narrow band FM to wide band FM. The narrow band FM has only the fundamental frequency. In our case this would be the 400 Hz or 500 Hz frequencies we used in the target. Second order harmonics begin to appear as the vibrational amplitude grows. This occurs because FM signal is a Bessel function with the parameter β . It can also occur from any nonlinearity in the vibrating surface. Wide band FM occurs when $\beta \cong 1$; therefore, the second harmonic will begin to appear when $\beta \cong 1$. The modulation index $\beta = 4\pi \frac{a}{\lambda}$. Here a equals the amplitude of vibration and λ equals the wavelength of laser light. The second harmonic begins to appear when

$$a \cong \frac{\lambda}{4\pi}. \quad (4-1)$$

The second harmonic should be to appear when the applied of vibration is approximately 844 nm. Therefore, the appearance of the second harmonic can give us a rough approximation of the amplitude of vibration without any complex processing required.

Similar estimates of larger amplitude vibrations can be made when the third harmonics are detected and etc.

2. System Improvements

The laser radar constructed was the first iteration of a design process and as such several lessons were learned. These lessons learned could yield a second iteration laser radar that would have better performance and be more robust.

The frequency discriminator was a commercial off the shelf model. Its sensitivity of 0.504 V/MHz was more ideally suited for much higher frequency modulation of the 30 MHz carrier wave. Our target was vibrating at much lower frequencies. A much higher sensitivity would be desired to improve the CNR for the system. This will require a specially designed frequency discriminator and limiter. If this is not possible, then amplifying the discriminator output signal (using a differential amplifier) is another possible solution. The resulting improvement can speed up signal processing times. Averaging techniques to improve the CNR would not be necessary and the system's ability to detect small target vibrational amplitudes would be improved as well.

The source of the power spectrum jump was never successfully tracked down. This interferes with the laser radar's ability to measure the target's vibrational amplitude. The target's vibrational amplitude can be approximated using the appearance of the second harmonic as described above. Accurate measurements of the target's actual velocity would also be required if the laser radar was to be used to determine vibrational amplitudes. Vibrational amplitudes may become very costly to calculate, requiring extensive algorithms to calculate the nonlinear function. Thus the approximation technique described above maybe the simplest way to quickly gain useful information on the amplitude of a particular vibrational frequency.

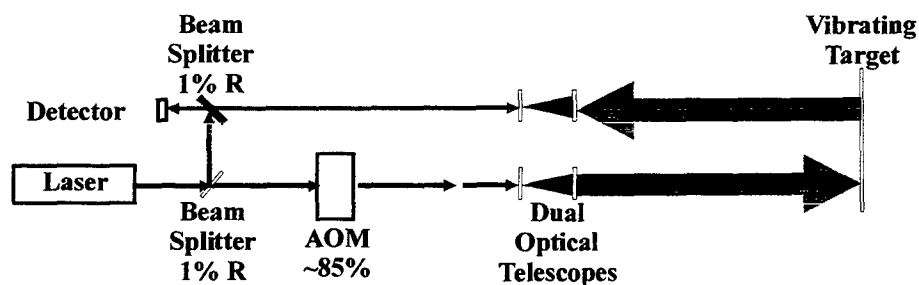
Range improvements can be made by using different optical beam splitters. The laboratory laser radar used a 53% reflective beam splitter to split off a reference or local oscillator beam. The idea was to closely match the intensity of the target beam and reference beam when they were recombined. This meant that a large portion of the laser's

power was wasted in the laboratory laser radar. For field use the reflected laser power from the distant target is much weaker and therefore does not require a strong local oscillator. A revised laser radar is shown in Figure 4-8. In this design a second telescope acting as collecting lenses has been added. The resulting efficiencies improve the theoretical range of the laser radar to 9.4 km at 10 Km visibility conditions.

Reducing the electronic bandwidth from MHz to kHz would also improve the range capabilities of the laser radar. SAW filters could be used instead of the less expensive LRC type filters. Ideally the filter systems should have a bandwidth of about 100 kHz. Our laser radar had a bandwidth of 6 MHz as a result of the frequency discriminator and filters used.

The detector we used was the least sensitive of the options available. Liquid nitrogen cooled HgCdTe detectors could be substituted to improve the sensitivity of the detector.

The U.S. Military continues to investigate the military applications of laser radar. This experiment has shown the possibility of using the laser radar as a means of detecting a target's vibrational signature. This signature can be used to identify vehicles and detect hidden or camouflaged vehicles and equipment. Perhaps the hardest part of the process remains signal processing and interpretation. Sonar and its ability to detect and identify targets under water are well known. That capability now exists for land systems. The work ahead will be to collect and identify land based systems by their acoustic signature.



$$\text{Optical Transmitting Efficiency} = (1-0.01)(0.85) = .84 \text{ or } 84\%$$

$$\text{Optical Receiving Efficiency} = (1-.01) = .99 \text{ or } 99\%$$

Figure 4-8 Improved Laser Radar Design

APPENDIX – LASER SAFETY PROCEDURES

Department of Physics
Naval Postgraduate School

1. Background. The Laser Radar Laboratory (Spanagel Room 018) will use various types of lasers to detect and classify various objects and gasses. It is intended that this laboratory will be modified at regular intervals to keep abreast with current technologies in this field.

The laboratory will house an I.R. laser. This laser is a 10 watt CO₂ 10.6 micron wavelength laser manufactured by Synrad. The laser is a Class IV laser that will be operated in the continuous wave mode. The laser is labeled "Danger" and the room will be developed to accommodate this laser.

2. Potential Hazards. Beam hazards for lasers must be of concern to all personnel operating the laser system. Where possible, the beams of the laser system will not be open to the casual observer.

a. Laser radiation entering the eye can cause permanent visual impairment or blindness. This hazard exists for both diffuse and specula reflections of a high power Class IV laser.

b. A fire hazard may exist if flammable materials are exposed to the direct laser beam.

c. Direct exposure of skin to the laser beam creates a potential for skin injury.

d. The greatest potential safety hazard is electrical shock from the power supply.

Besides the beam, the power supply for the laser presents a potential source for electrocution. Laser power supplies are not to be opened by other than trained personnel. Additionally, in all applications, the laser must be operated with minimum power. In case of power failure, the laser will be put in the "off" or "stand-by" modes until the sources of electricity has returned.

3. Administrative Requirements

a. In order to be an authorized laser user, an individual must:

1. Have received a slit lamp laser user's eye exam from a qualified examiner at the DLI Heath Clinic (Military) or the Occupational Health Clinic (Civilian) prior to commencing laser use.

2. Have received documented laser safety orientation from the Physics Department Laser Safety Officer (Mary Atchley).

b. Upon completion of the laser project, undergo a termination eye exam.

4. Safety Procedures.

a. DO NOT LOOK DIRECTLY INTO THE LASER BEAM.

b. No lasers shall be operated such that the beam is visible to the casual observer.

c. A laser warning sign will be posted at the entrance to the room. This sign will comply with NAVPGSCOLINST 5100.2D and ANSI Z136.1 -1993.

d. No laser shall be operated without a method to positively interrupt the beam.

e. No laser shall be operated without sufficient safety goggles for all persons in the laboratory. (Note: the goggles must be of the types approved for the laser in operation, i.e. specific to the laser wavelength and of sufficient optical density.

f. No laser shall be operated without erecting appropriate barriers or warning tape around the laser area.

g. No laser shall be operated which has had any of the manufacturer's safety interlocks defeated.

h. Laser beams will not be directed at an arbitrary target. If the primary target is not used, a "light-dump" will be used.

i. The laser will not be aimed at the door area of room 018.

5. Standard Operating Procedures. The checklist for covering safety and start up procedures for the 10 watt Synrad laser are as follows:

___ a. Work must be done with a partner to ensure safety.

___ b. Ensure the "Danger" Sign is posted on the external side of the door to room 018.

___ c. Check to make sure the outside warning light is working when the door to room 018 is closed.

- ___ d. Check to make sure the interlock box is operating correctly. The green light should come on when the door to room 018 is closed. It should turn off when the door is opened.
- ___ e. Inspect the electrical connections of all equipment and ensure that flammable materials are cleared from the area. Check the equipment and grounds for proper connections (no loose wiring or clutter should be present).
- ___ f. Verify the fire extinguisher is within arms reach of the operating area and is serviceable.
- ___ g. Clear the laser area of any reflective materials not involved with the experiment.
- ___ h. Be sure the door to room 018 is closed and unlocked.
- ___ i. Align optical components as much as possible before turning the laser on.
- ___ j. Only trained persons involved with the experiment should be in the laser area.
- ___ k. Ensure everyone in the room is wearing the proper goggles.
- ___ l. Ensure an adequate beam dump is placed at the end of the light path.
- ___ m. Advise everyone the laser is now being turned on.
- ___ n. Verify all electrical and cooling interconnections have been accomplished according to manufacturer instructions.
- ___ o. Set the mechanical shutter on the laser to the ON (open) position.
- ___ p. Set the external DC power supply switch to ON position.
- ___ q. Verify that the PWR LED on laser illuminates.
- ___ r. Turn laser key switch to ON position and/or close the remote interlock. Verify green PWR LED on laser illuminates.
- ___ s. Turn on control voltage supply (5 volt supply). Verify that the red LASE LED on laser illuminates after five seconds.
- ___ t. Turning off the laser is accomplished by turning off laser power(set keyswitch to off or open remote interlock as appropriate).
- ___ u. Turn off power supply to the laser and the control voltage.

____ v. Set the mechanical shutter to closed or OFF position.

6. Emergency procedures.

Fire. Turn the power to the system using the quickest means (Emergency shut off can be accomplished by turning the interlock box power off or turning the power strip switch off.)

Do not attempt to extinguish the fire alone. Contact the fire department.(x2333) The fire alarm handle is located next to room 007 of Spanagel Hall. Use the fire extinguisher to control the fire until the fire department arrives.

Injury. Turn off the laser by any of the following means:

Turn off the interlock switch.

Turn off the power supply switch.

Turn off the control voltage.

Turn the interlock key to off.

The laser light can also be blocked temporarily by closing the mechanical shutter. The non injured person should then transport the injured person to the nearest medical facility to receive medical treatment.

Always notify the Laser Safety Officer (x2649) or laboratory manager if you have been injured or suspect that you may have been injured by the laser beam.

In the event that any irregularities in the operation of the laser arise, mechanical, optical or electrical, shut down the system immediately and notify the cognizant professor as soon as possible.

LIST OF REFERENCES

American National Safety Institute, ANSI Z136.1-1936, American National Standard For Safe Use of Lasers, The Laser Institute of America, New York, New York, 1993.

Chance, Thomas H., FM-CW Laser Radar at 10.6 Microns, Naval Postgraduate School Thesis, Monterey, California, 1974.

Chang, I.C., "Acousto-optic Devices and Applications," IEEE Transactions on Sonics and Ultrasonics, Vol. SU-23, No. 1, January 1976.

Fraunfelder, A. Jr., A Heterodyne Detection FM-CW Laser Radar Using a 10.6 μ Source, Naval Postgraduate School Thesis, Monterey, California, 1974.

Harney, Robert C., Laser Radar Systems: Theory, Technology, & Applications, Lecture Notes, Orlando Florida (now Monterey, California), 1993.

Harney, Robert C., The Rate Equation Theory of Lasers, Naval Postgraduate School Class Notes, Monterey, California, 1996.

Harney, Robert C., Sensor and Devices, Naval Postgraduate School Class Notes, Monterey, California, 1996.

Hawkes, John and Latimer, Ian, Lasers: Theory and Practice, Prentice Hall International, New York, New York, 1995.

Haykin, Simon, Communication Systems, 3rd Edition, John Wiley & Sons, Inc., New York, New York, 1994.

Hecht, Eugene, Optics, 2nd Edition, Addison-Wesley Publishing Company, Inc., 1987.

Hecht, Jeff, The Laser Guidebook, 2nd Edition, McGraw-Hill Inc., New York New York, 1992.

Iga, Kenichi, Fundamental of Laser Optics, Plenum Press, New York, New York, 1994.

Interaction Corp., Acousto-optic Modular Instruction Manual, Interaction Corp., Bellwood, Illinois, 1996.

Interaction Corp., Model Ge-3030 Modulator Driver Instruction Manual, Interaction Corp., Bellwood, Illinois, 1996.

Jelalian, Albert V., Laser Radar Systems, Artech House, Norwood Massachusetts, 1992.

Kranz, Wolfgang, "Target Classification by Laser Vibration Sensing," Fifth Conference on Coherent Laser Radar: Technology and Applications, Society for Optical Engineering (SPIE) Volume 1181, The International Society for Optical Engineering, Bellingham, Washington, 1989.

Melles Griot Inc., Optics, Opto-Mechanics, Lasers, Instruments Catalog, Melles Griot Inc., Irvine, California, 1995/1996.

Miteq, Test Data Sheets on MITEQ Model N. FMDM-30/6-8B and Model LCPM-30/10-70B, Miteq, Hauppauge, New York, 1996.

Mini-Circuits, RF/IF Designer's Handbook, Mini-Circuits, Brooklyn, New York, 1996.

Physik Instrumente, Products for Micropositioning Catalog, Polytec PI, Inc., Costa Mesa, California, 1996.

Renhorn, Ingmar et al, "Coherent laser Radar for Vibrometry: Robust Design and Adaptive Signal Processing," Applied Laser Radar Technology II, Society for Optical Engineering (SPIE) Volume 2472, The International Society for Optical Engineering, Bellingham, Washington, 1989.

Schlessinger, Monroe, Infrared Technology Fundamentals, 2nd Edition, Marcel Dekker Inc., New York, New York, 1995.

Scruby, C. B., and Drain, L. E., Laser Ultrasonics: Techniques and Applications, Adam Hilger, Bristol, England, 1990.

Schwartz Electro-Optics Inc., Final Technical Report on Non-cooperative Combat Identification, prepared for: Department of the Army, U.S. Army CECOM Night Vision and Electro-Optics Directorate, Fort Belvoir, Virginia, 1994.

Seigman, Anthony E., An Introduction to Lasers and Masers, McGraw-Hill Book Company, New York, New York, 1971.

Seigman, Anthony E., Lasers, University Science Books, Sausalito, California, 1986.

Shrader, Robert L., Electronic Communication, 6th Edition, Glencoe Division of Macmillan/McGraw-Hill, Westerville, Ohio, 1991.

Skolink Merrill L., Introduction to Radar Systems, 2nd Edition, McGraw-Hill, Inc., New York, New York, 1980.

Synrad Inc., Series 48 Lasers: Operation and Service Manual Version 2.1, Synrad Inc., Mukilteo, Washington, 1996.

Taub, Herbert and Schilling, Donald, L., Principles of Communication Systems, 2nd Edition, McGraw-Hill Publishing Company, New York, New York, 1986.

Thor Labs Inc., Opto-Mechanics Catalog, Thor Labs Inc., Newton, New Jersey, 1996/1997.

Technical Manufacturing Corporation (TMC), Vibration Solutions, General Catalog, Technical Manufacturing Corporation, Peabody, Massachusetts, 1995/1996.

Verdeyen, Joseph T., Laser electronics, 3rd Edition, Prentice Hall, Englewood Cliffs, New Jersey, 1995.

Wilson J. and Hawkes J. F. B., Optoelectronics, An Introduction, 2nd Edition, Prentice Hall, New York, New York, 1989.

INITIAL DISTRIBUTION LIST

1. Defense Technical Information Center.....2
8725 John J. Kingman Rd., STE 0944
Ft. Belvoir, VA 22060-5101
2. Dudley Knox Library.....2
411 Dyer Road
Naval Postgraduate School
Monterey, CA 93944-5101
3. Chairman, (Code PH).....1
Department of Physics
Naval Post Graduate School
Monterey, CA 93943-5117
4. Professor Robert C. Harney (Code PH/Ha).....3
Naval Post Graduate School
Monterey, CA 93940
5. Professor Andres Larraza (Code PH/La).....2
Naval Post Graduate School
Monterey, CA 93940
6. CPT James V. Day.....2
2161 Stagecoach Road
Placerville, CA 95667